

# POLITECNICO DI TORINO

**Corso di Laurea Magistrale in Ingegneria Meccanica**

**Tesi di Laurea Magistrale**

**Study of the influence of the type of root profile on  
tooth bending stresses in spur gear drives**



**Relatori:**

Nicola Bosso

Ignacio González Pérez

**Candidato:**

Stefania Rosato

**Ottobre 2020**

# Contents

<b>1</b>	<b>Introduction</b>	<b>1</b>
1.1	Introduction . . . . .	1
1.2	Objectives . . . . .	1
1.3	Work structure . . . . .	2
<b>2</b>	<b>State of the Art</b>	<b>3</b>
2.1	Introduction . . . . .	3
2.2	Hermite curve . . . . .	3
2.3	Elliptical curve . . . . .	10
2.4	Bezier curve . . . . .	15
<b>3</b>	<b>Fundamentals</b>	<b>20</b>
3.1	Introduction . . . . .	20
3.2	Modeling of an elliptical curve . . . . .	20
3.3	Modeling of a Hermite curve . . . . .	22
3.4	Modeling of a Bezier curve . . . . .	23
<b>4</b>	<b>Methodology</b>	<b>26</b>
4.1	Procedure for the analyses . . . . .	26
<b>5</b>	<b>Results</b>	<b>36</b>
5.1	Numerical examples . . . . .	36
5.2	ISO profile A . . . . .	41
5.3	ISO profile B . . . . .	45
5.4	ISO profile C . . . . .	48
5.5	ISO profile D . . . . .	52
<b>6</b>	<b>Conclusions</b>	<b>56</b>

# Chapter 1

## Introduction

### 1.1 Introduction

Spur gear drives are widely applied for power transmission between parallel shafts. Their performance is affected mainly by two types of failure. One is related with the pitting of the contacting tooth surfaces. The other one is related with the tooth brake through bending. This Master Thesis is directed to the improvement of the behavior of spur gear drives related with the second type of failure, tooth brake through bending. For doing that, a study of the influence of the type of root profile on tooth bending stresses in spur gear drives is presented.

Different types of root profiles will be applied through the use of the Integrated Gear Design (IGD) software developed by the Research Group of Advanced Gear Transmissions of the Universidad Politécnica de Cartagena. Standardized ISO profiles will be implemented considering types A, B, C and D of this Standard. The type of root profile that the Standard considers is a trochoid, that is a curve generated by a rounded tip of the rack-cutter tooth. Then, this conventional root profile will be substituted by three types of root profile considering elliptical, Hermite and Bezier curves. Besides the type of the root profile, the effect of their dimensions on bending stresses are also investigated by decreasing the root diameter, increasing the fillet-form diameter, or reducing the root land.

Furthermore, with the same software, bending stresses will be analyzed on the root profiles, through the finite element method. Using the finite element models that are exported from IGD and using a general purpose software for finite element analysis (ABAQUS), bending stress will be compared and the appropriate conclusions will be drawn.

### 1.2 Objectives

The objective of this thesis work is to investigate the influence of different types of root profiles on bending stresses in spur gear drivers. The main objectives of this thesis work are:

- (1) Comparison of bending stresses at the base of the tooth considering different standardized ISO profiles;
- (2) Comparison of bending stresses at the base of the tooth with elliptical base profile and by reducing the root radius, increasing the fillet-form radius, or reducing the root land;
- (3) Comparison of bending stresses at the base of the tooth with Hermite base profile and by reducing the root radius, increasing the fillet-form radius, or reducing the root land;
- (4) Comparison of bending stresses at the base of the tooth with a third-degree Bezier base profile and by reducing the root radius, increasing the fillet-form radius, or reducing the root land;

The type of stress that will be considered for comparison of bending stresses will be the maximum principal stress since it is the most representative stress in bending.

## 1.3 Work structure

The following thesis work is structured in the following chapters:

- Chapter 1. Introduction.
- Chapter 2. State of the Art.
- Chapter 3. Fundamentals.
- Chapter 4. Methodology.
- Chapter 5. Results.
- Chapter 6. Conclusions.

In Chapter 1, an introduction of the topic to be analyzed throughout the present thesis project is presented and the objectives are outlined.

In Chapter 2, the state of the art related with the improvement of bending behavior in gear drives is reported through the description of other publications on this subject.

In Chapter 3, the applied theory to carry out the following thesis project is reported. The theoretical foundations are presented.

In Chapter 4, the methodology that have been applied during the course of the various tests is reported.

In Chapter 5, the obtained results are reported and are compared with each other.

In Chapter 6, the appropriate conclusions are drawn.

## Chapter 2

# State of the Art

### 2.1 Introduction

In this chapter, the effects of fillet geometry on bending stresses of spur gears that have been investigated in previous publications are presented. Reference [1] starts describing the main parts of the gear tooth surface (see Figure 2.1.1). It consists of four parts:

- 1. Top land;
- 2. Active tooth surface;
- 3. Fillet tooth surface;
- 4. Root land.

The top land is the part of external surface that is located at the top of a gear tooth. The active tooth surface is where the bearing contact between pinion and gear occurs. Contact patterns are always developed and represented on the active tooth surface and it is where contact stresses are obtained. The fillet is the portion of the gear tooth surfaces that joins the active tooth surface with the root land. The geometry of the fillet gear tooth surface is obtained as a result of the process of gear generation. This is where maximum bending stresses are obtained. Root land is the portion of the surface that joins the fillets of two consecutive gear teeth.

In the following thesis work the curve that is used in the fillet is modified to try to decrease bending stresses. The peculiar characteristics of each curve used in the modeling of the present work will be described.

### 2.2 Hermite curve

The first curve that is described is the Hermite curve. The fillet geometry joins the lower boundary of the active gear tooth surface with the root land and the initial and final tangent vectors can be

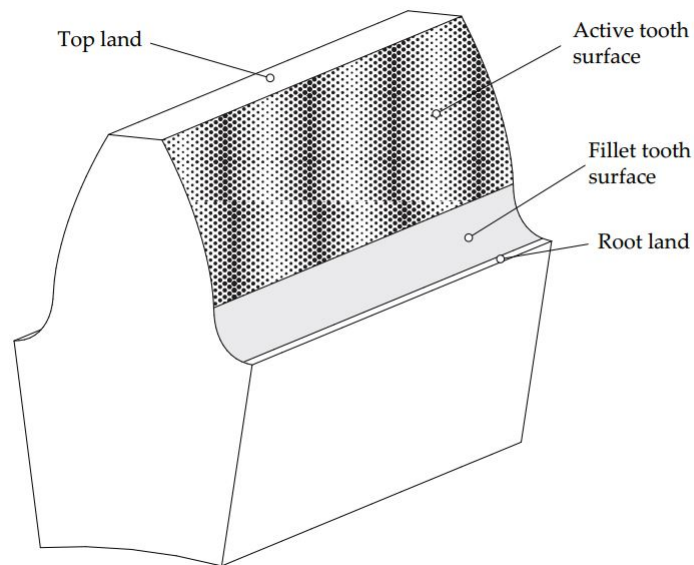


Figure 2.1.1: Gear tooth parts (source in [1])

considered as known all over the upper and lower boundary of the fillet surface. Hermite curves are very suitable for providing the fillet geometry [1] on those manufacturing processes where there is not a cutting action (forging, 3D-printing).

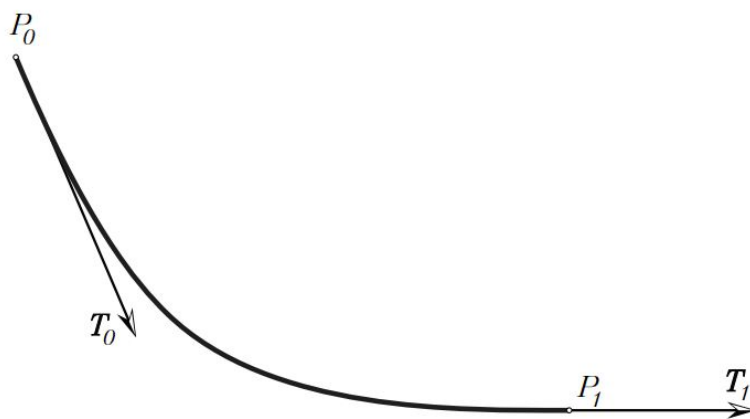


Figure 2.2.2: Basic data of a Hermite curve (source in [1])

Hermite curves are defined by two points  $P_0$  and  $P_1$  and two tangent vectors  $\mathbf{T}_0$  and  $\mathbf{T}_1$  (see Figure 2.2.2). The Hermite curve between those points is defined by:

$$r(t) = (2t^3 - 3t^2 + 1)P_0 + (-2t^3 + 3t^2)P_1 + (t^3 - 2t^2 + t)T_0 + (t^3 - t^2)T_1 \quad (2.2.1)$$

where  $0 \leq t \leq 1$ . The blending functions are:

$$b_1 = 2t^3 - 3t^2 + 1 \quad (2.2.2)$$

$$b_2 = -2t^3 + 3t^2 \quad (2.2.3)$$

$$b_3 = t^3 - 2t^2 + t \quad (2.2.4)$$

$$b_4 = t^3 - t^2 \quad (2.2.5)$$

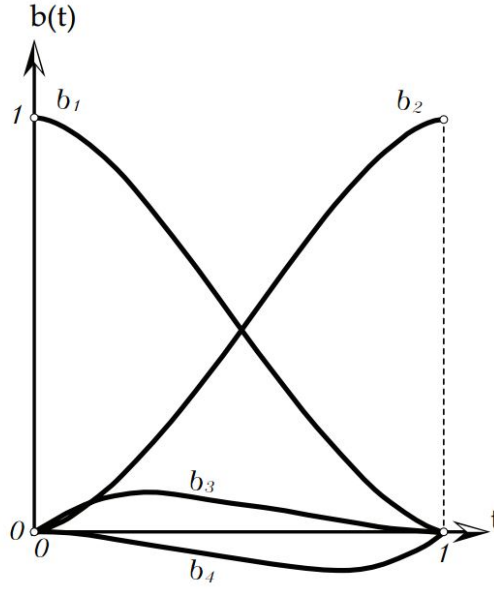


Figure 2.2.3: Blending functions for Hermite curves (source in [1])

Figure 2.2.3 shows a graph of the blending functions for Hermite curves where the influence of each of the given points and vectors as a function of the parameter  $t$  along the curve can be observed. These functions show the effect of the given initial and final points as well as the tangent vectors. For modeling the fillet of a gear tooth, the coordinates of point  $P_0$ ,  $P_1$ ,  $T_0$  and  $T_1$  be denoted as  $(x_{P_0}, y_{P_0}, z_{P_0})$ ,  $(x_{P_1}, y_{P_1}, z_{P_1})$ ,  $(x_{T_0}, y_{T_0}, z_{T_0})$  and  $(x_{T_1}, y_{T_1}, z_{T_1})$ . The coordinated of a point  $P$  of the fillet will be obtained:

$$x_P(t) = b_1 x_{P_0} + b_2 x_{P_1} + b_3 x_{T_0} + b_4 x_{T_1} \quad (2.2.6)$$

$$y_P(t) = b_1 y_{P_0} + b_2 y_{P_1} + b_3 y_{T_0} + b_4 y_{T_1} \quad (2.2.7)$$

$$z_P(t) = b_1 z_{P_0} + b_2 z_{P_1} + b_3 z_{T_0} + b_4 z_{T_1} \quad (2.2.8)$$

The modules of tangents  $T_0$  and  $T_1$  were kept equal.  $T_0$  has been obtained as the tangent at the lower point of the active tooth profile, then normalized and multiplied by the corresponding tangent

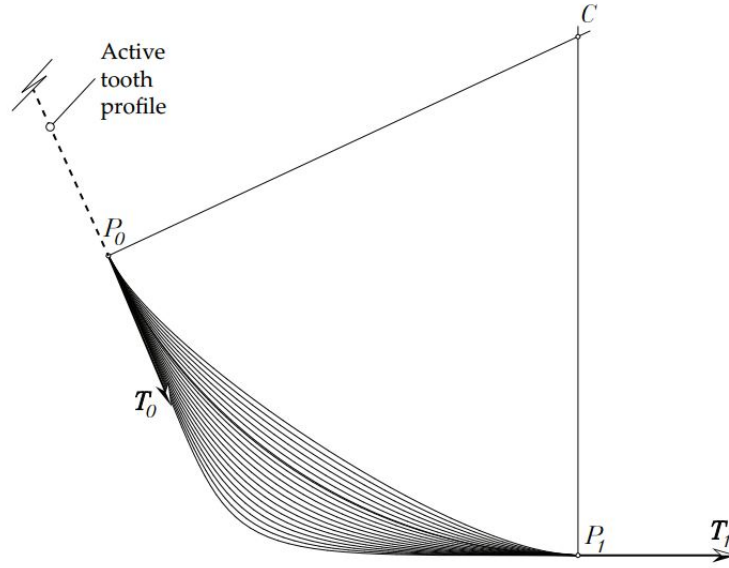


Figure 2.2.4: Different possible geometries for the fillet by using Hermite curves (source in [1])

weight  $t_0$  and the module  $m$  of the gear drive.  $T_1$  has been obtained as the tangent to the root circle at  $P_1$ , and normalized and multiplied by the corresponding tangent weight  $t_1$  and the module  $m$  of the gear drive. The finite element method has been used to perform stress analysis for all cases of design that are described in [1]. Finite element comprising five pairs of contacting teeth have been employed to avoid influence of the boundary conditions on the results. Three-dimensional solid element model of type C3D8I have been used, being hexahedral first order elements enhanced by incompatible deformation modes in order to improve their behavior. Pinion and gear materials are steel defined with elastic modulus of 210 GPa and Poisson ratio of 0.3.

In the article mentioned above, there is an experiment for investigation of the effect of fillet geometry for the fillet tooth surface of spur gears. The procedure used to predict the root stresses of the gears incorporates the geometry shown in Table 2.2.1.

The stress analysis for the trochoidal gear tooth fillet, as generated by a rack cutter with an edge radius coefficient of 0,38 has been studied. The maximum bending stress at the fillet surface is 259 MPa, for this case where the fillet is a product of the generating process. A total of 25 cases of design were considered in this study comprising 5 different values of the initial tangent weight  $t_0$  from 0,7 to 1,1 with a step equal to 0,1 in combination with the same 5 values for the final tangent weight  $t_1$  of the Hermite curve. The evolution of maximum contact and bending stresses is obtained so that the maximum value of the stress along the cycle of meshing of the gear is always obtained. In the Figure 2.2.6, the gear tooth fillets for three cases of design were  $t_0 = t_1 = 0,7$ ,  $t_0 = t_1 = 0,9$  and  $t_0 = t_1 = 1,1$ . The lower the tangent weight is, the more gentle connection from the active tooth surface and the root surface is made (lower curvature at the middle of the root



Figure 2.2.5: Finite element model with five pair of contacting teeth (source in [1])

profile).

In the Figure 2.2.7, the 3D surface plot of the bending stress at the gear tooth fillet for 25 different combinations of tangent weights, varying from 0,7 to 1,1, is shown. Notice that the bending stress are reduced considerably for the lower values of tangent weights. We notice that given a tangent weight  $t_0$  for lower stresses, the value of  $t_1$  should be as lower as possible. Tangent weight  $t_0$  should be obtained mainly considering the avoidance of tip-fillet interference.

In the Figure 2.2.8, a contour plot of contact stresses as a function of the tangent weights is shown.

A maximum bending stress of  $\sigma_b=313,36$  MPa is obtained when considering  $t_0 = t_1 = 1,1$ . A maximum bending stress of  $\sigma_b=243,36$  MPa is obtained when considering  $t_0 = t_1 = 0,7$ . In

Table 2.2.1: Data considered in [1]

Parameter	Pinion	Gear
Number of teeth	21	34
Module [mm]	2,5	2,5
Addendum coefficient	1,00	1,00
Dedendum coefficient	1,25	1,25
Profile shift coefficient	0,18292	-0,18292
Face width [mm]	19	19
Normal pressure angle [deg]	20	20
Center distance [mm]	68,75	
Edge radius coefficient	0,38	0,38
Young's Modulus [GPa]	210	210
Poisson's ratio	0,3	0,3
Applied Torque [Nm]	175	

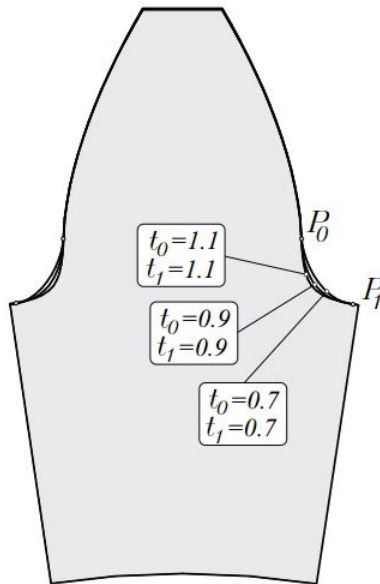


Figure 2.2.6: Comparison of geometries of fillets for a pinion (source in [1])

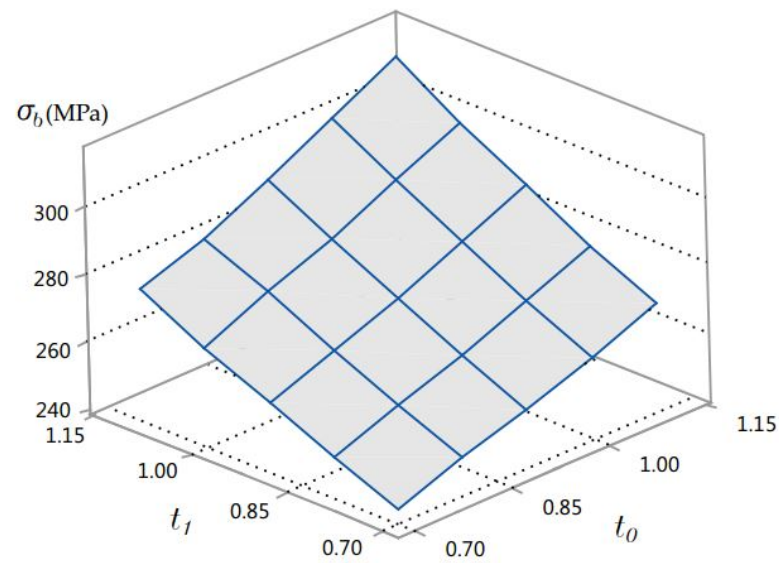


Figure 2.2.7: 3D surface plot of bending stresses as a function of tangent weights (source in [1])

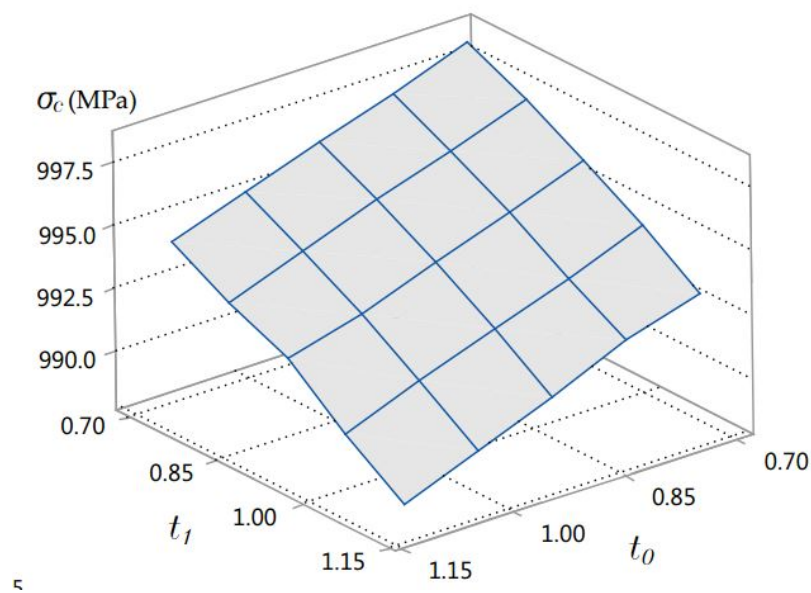


Figure 2.2.8: 3D surface plot of contact stresses as a function of tangent weights (source in [1])

conclusion, the fillet geometry has an important influence on bending stresses. Hermite curves have been used as fillet geometry and by considering lower values of tangent weights, a reduction of bending stress as high as 22,3% has been obtained with respect to the maximum value corresponding to higher values of tangent weights. Contact stresses are influenced as well by the geometry of the fillet although such influence can be neglected. Modeling of fillet geometry by Hermite curves is an efficient way to provide gear geometric models with fillets when the surfaces are not designed to be generated by a cutting or grinding tool.

## 2.3 Elliptical curve

Reference [2] presents an elliptical mathematical shape that allows one to specify the root radius as well as the start of the ellipse along the profile. Once one has reached the gear pair design stage, it will be necessary to check for the effect on the mating tooth of such a root because that is a major danger. Reference [2] uses two user-defined parameters, the root circle radius  $R_r$  and the radius  $R_A$  at which the circular root profile is tangent to the involute profile, a requirement to define a root shape that is elliptical. With point A at  $(x_A, y_A)$  representing the start of root geometry at radius  $R_A$  and point C at  $(x_C, y_C)$  representing the root center, the following conditions are imposed to fit a portion of an ellipse between points A and C:

- 1. The root fillet curve  $y_f(x)$  and the involute profile  $y_{inv}(x_A)$  must intersect at point A at radius  $R_A$  such that

$$y_{inv}(x_A) = y_f(x_A) = y_A \quad (2.3.9)$$

- 2. The root fillet curve  $y_f(x)$  and the involute profile  $y_{inv}(x)$  must have the same slope at point A such that:

$$\frac{dy_{inv}(x)}{dx}(x_A) = \frac{dy_f(x)}{dx}(x_A) \quad (2.3.10)$$

- 3. The root fillet curve  $y_f(x)$  and the root circle  $y_r(x)$  must intersect at the root center C at radius  $R_r$  such that:

$$y_f(x_C) = y_r(x_C) = y_C \quad (2.3.11)$$

- 4. The root fillet curves  $y_f(x)$  and the root circle  $y_r(x)$  must have the same slope at the root center C such that:

$$\frac{dy_f(x)}{dx}(x_C) = \frac{dy_r(x)}{dx}(x_C) \quad (2.3.12)$$

A portion of an ellipse is defined to meet these four conditions such that one of the principle axes of the ellipse is on the  $y$  axis. Various shapes of ellipses can be fit by simply varying  $R_A$  for a given values of  $R_r$  [2].

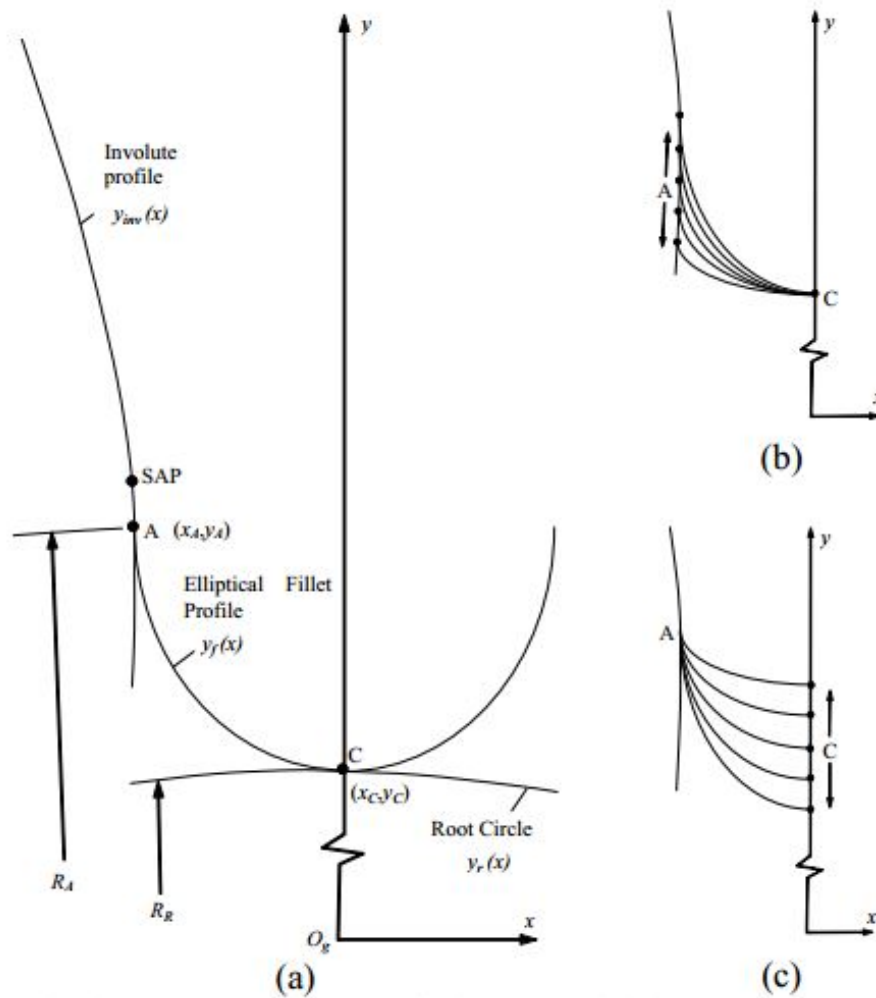


Figure 2.3.9: (a) Parameters defining an elliptical root geometry, (b) various root geometries obtained by varying with constant, and (c) various root geometries obtained varying with constant (source in [2])

In the article mentioned above, there is an experiment for investigation of the effect of fillet geometry for the fillet tooth surface of spur gears. The procedure used to predict the root stresses of the gears incorporates the geometry below:

- Number of Teeth=34;
- Module=4,233 mm;
- Helix Angle=0 deg;
- Outside Diameter=152,40 mm;

- Root Diameter=131,75 mm;
- Face Width=25,40 mm;
- Transverse Tooth Thickness=6,57 mm;
- Diameter at Thickness Measurement=143,93 mm;
- Young's Modulus=210 GPa;
- Poisson's Ratio=0,30;

Using the basic test gear design defined in this table, by generating different tooth root profile a parametric study was performed by keeping the root radius constant at  $R_r=65,87$  mm and varying  $R_A$  within a range below the start of the active profile.

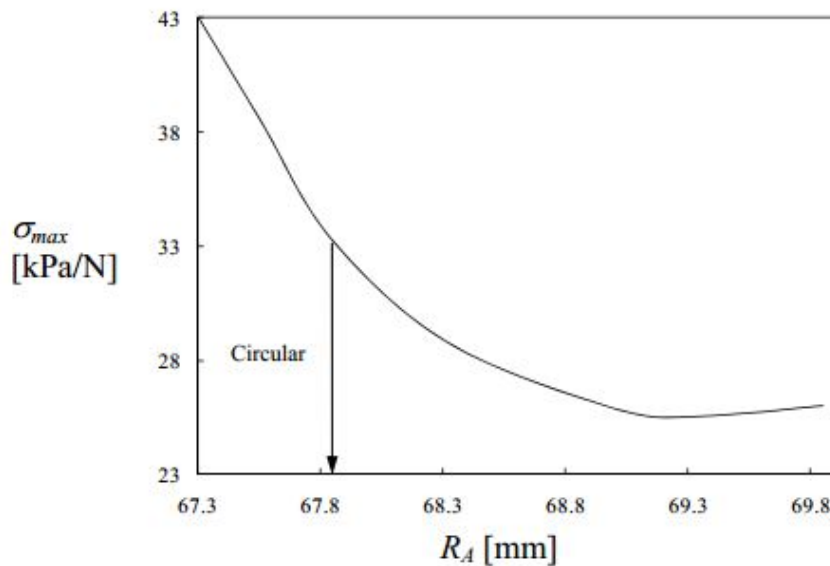


Figure 2.3.10: Variation of the maximum root stress with  $R_A$  of the example gear design with  $R_r=65,87$  mm (source in [2])

Figure 2.3.10 shows the variation of the maximum root stress  $\sigma_{max}$  as a function of  $R_A$  with the tooth loaded by a unit load at a radius of 75,15 mm. In the experiment, it is seen that  $R_A=67,85$  mm corresponding to a full circular root profile does not result in the lowest  $\sigma_{max}$  values. For four of these root profiles under the same loading conditions, it is shown in Figure 2.3.11 a distribution of root stress values as a function of the radial position  $R$ . It is seen that the maximum stress values are decreased with increased  $R_A$  values while, at the same time, the  $R$  at which  $\sigma_{(R)} = \sigma_{max}$  is reduced.

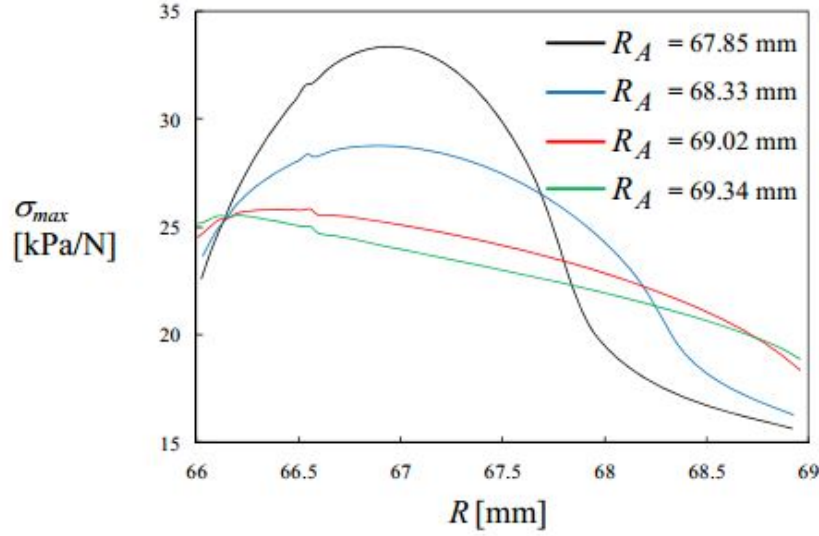


Figure 2.3.11: Root stress evolution along the root profile for four root profiles given a unit load applied at a radius of 75,15 mm (source in [2])

While the  $R_A=67,85$  mm and unit load locations are kept constant, the value of root circle radius  $R_r$  of the example gear is varied. Figure 2.3.12 shows the variation of the maximum root stress  $\sigma_{max}$  as a function of  $R_r$ .  $R_r=65,87$  mm corresponds to a full circular root profile with  $\sigma_{max}=33,33$  kPa/N. The elliptical profiles with  $R_r > 65,87$  mm have lower values.

The basic test gear geometry is a symmetric tooth design with 20 degree pressure angle on each flank. Asymmetric tooth geometries are introduced and compared to the symmetric designs with both circular and elliptical root profiles. A set of asymmetric tooth designs is obtained by fixing the pressure angle of one flank to observe the influence of varying the pressure angle of the coast side. The second group of analysis loads the flank where pressure angle is varied. Figure 2.3.13 shows several tooth profiles with 20 pressure angle on the right hand side of tooth and various pressure angle on the left hand side of the tooth. The minimum pressure angle used for the coast side was 15 degrees. The maximum pressure angle used for the coast side was 28,8 degrees. All design variation have full circular profiles on both drive and coast side.

Figure 2.3.14 shows a comparison of  $\sigma_R$  distributions for these asymmetric tooth designs with the input load applied at a radius of 75,15 mm. The figure shows that the peak stress increases when the pressure angle is reduced and decreases for increasing coast side pressure angle.

The combination of an optimal root shape for the drive side and a larger coast side pressure angle was shown to deliver a root stress reduction greater than with either of two concepts used separately. The boundary element root stress prediction procedure was shown to predict stresses at the gage location accurately for both symmetric and asymmetric tooth profiles with various fillet

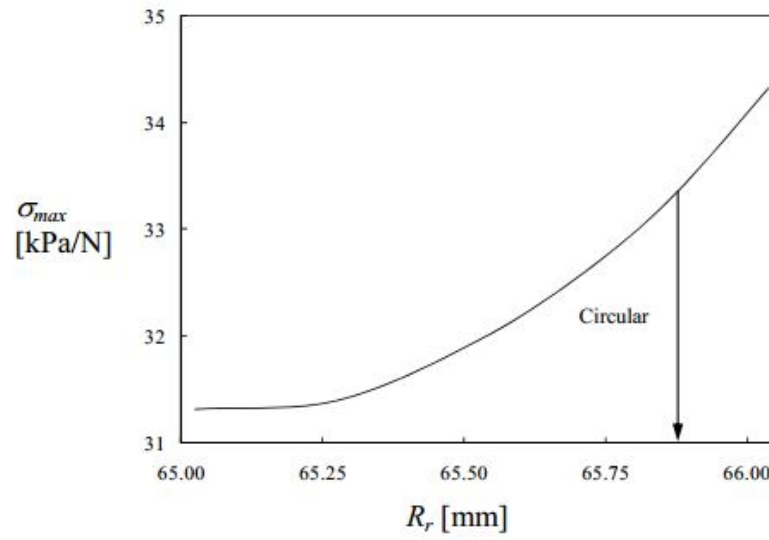


Figure 2.3.12: Variation of the maximum root stress with  $R_r$  of the example gear design with  $R_A = 67,85$  mm (source in [2])

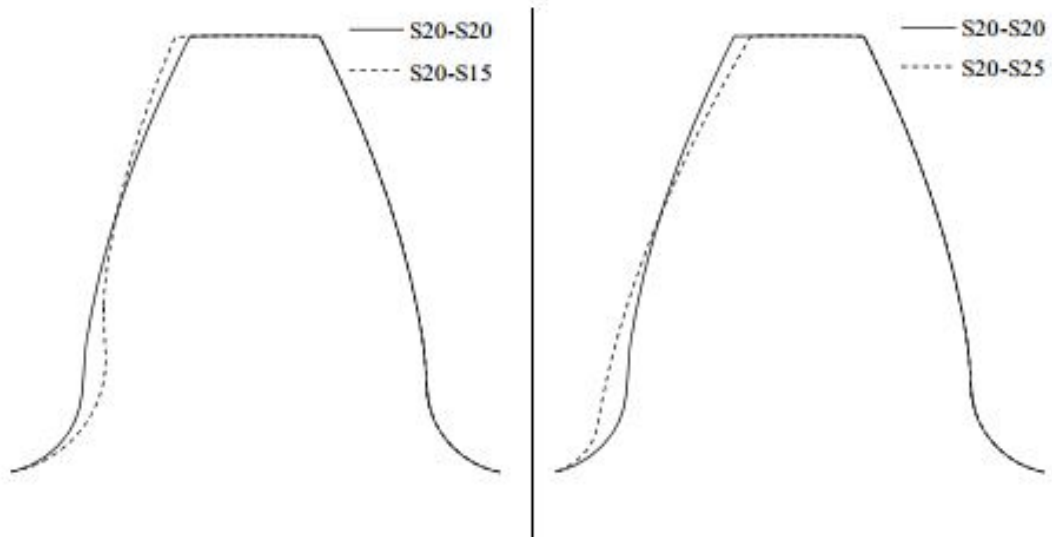


Figure 2.3.13: Samples of asymmetric teeth (source in [2])

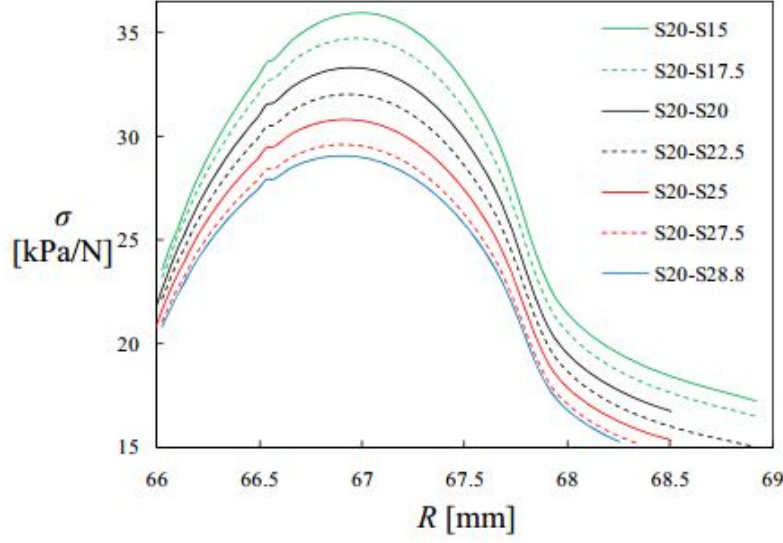


Figure 2.3.14: Root stress for a series of asymmetric designs (source in [2])

geometries. In conclusions, prediction and experiment presented confirm that the fillet geometry is a primary factor impacting the bending stress of a gear tooth. An elliptical root shape can be used to create larger fillet curvatures that can yield lower stresses than the corresponding best design practice using the largest possible circular root fillet. Each gear size will have a unique, optimum elliptical shape, however one must check for possible tooth interference prior to applying the elliptical shape. There exists a unique circular fillet profile that has the maximum radius, based on the values of the root circle radius and the radius at which the root fillet starts. The predictions and measurements from this study indicate that elliptical geometries with lower stresses usually exist, while this geometry represents the best of circular root geometries.

## 2.4 Bezier curve

The Bezier curves was developed by the French engineer Pier Bezier in 1960 [3]. The definition of a cubic Bezier curve occurs by the four control points  $P_0$ ,  $P_1$ ,  $P_2$  and  $P_3$ , where  $P_0$  is the starting point and  $P_3$  is the end point. The curve is created by connecting the points and repeatedly linking the ensuing distances at equal length conditions (see Figure 2.4.15).

The mathematical description of the cubic Bezier curve is:

$$\vec{B}(t) = \sum_{i=0}^3 (3, i) t^i (1-t)^{3-i} \vec{P}_i \quad (2.4.13)$$

In this context, the control variable  $t$  depicts the progression of the Bezier curve within its

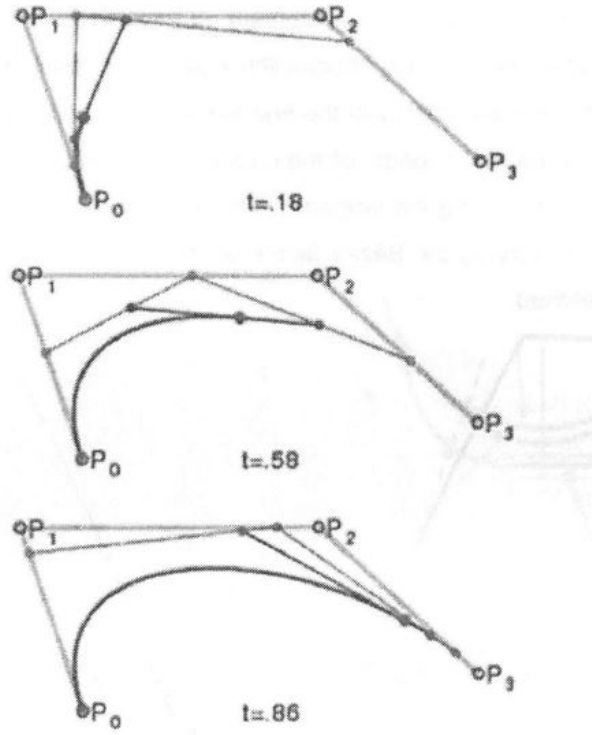


Figure 2.4.15: Creation of a cubic Bezier curve (source in [3])

definition range  $t \in [0, 1]$ .  $P_i$  is the direction vector of the support point. The point  $P_0$  and  $P_3$  mark the start and the end of the Bezier curve and consequently the transition into the gear root, and this has influence on the root geometry and thus on the load capacity. The points  $P_0$  and  $P_3$  must be situated on the tangents of the starting and the end point. The risk of possible meshing interferences by a collision of the tooth tip with the root of the opposing gear must not be ignored. The localization of these points has been described as transition diameter  $d_u$ , which has to be selected in such a way that the optimized root contour allows the trace of the counter gear tip to have clearance. The parametrization of a Bezier root fillet requires only one quantity which is called Bezier factor  $Be$  (see Figure 2.4.16). The distance of point  $P_1$  and  $P_2$  to the intersection of the tangents is used with the orthogonal cathetus of the first tension triangle. This distance is the product of the Bezier factor  $Be$  and the length of the cathetus of the deepest triangle. By moving the control points  $P_1$  and  $P_2$  along the tangent in the direction of the gear tip or downwards to the wheel axle, or by varying the Bezier factors  $Be$ , the gear root contour is correspondingly compressed or stretched [3].

Figure 2.4.17 shows the comparison depicted of a classic root fillet with a bionic one and the newly defined Bezier root contour between the two newer gear root geometries. The difference to the classic gear root contour is evident. The shape of the new geometry suggests a distinctly

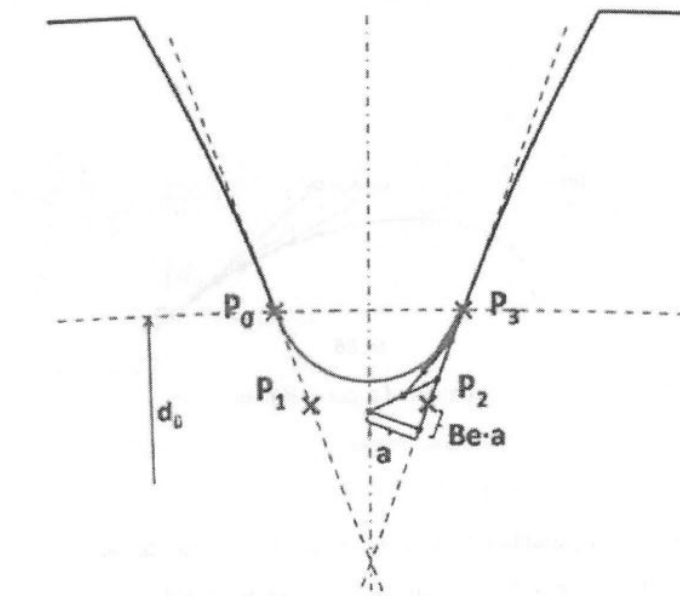


Figure 2.4.16: Figure of gear tooth (source in [3])

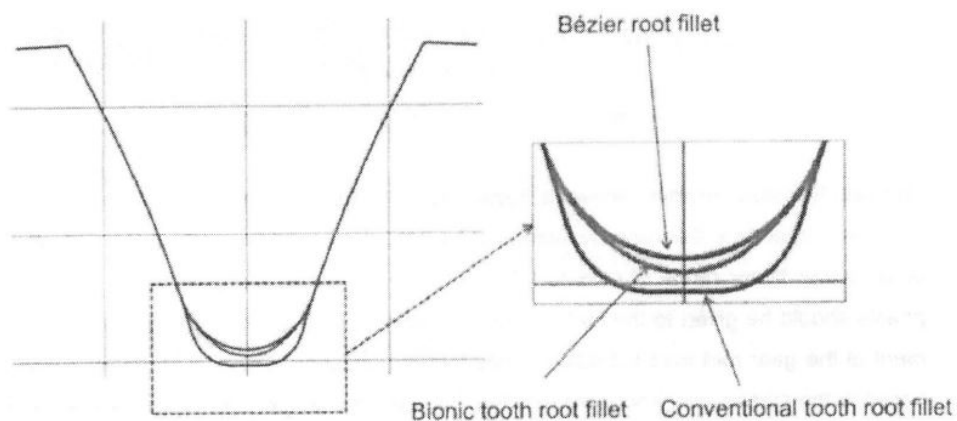


Figure 2.4.17: Comparison of different gear root geometries (source in [3])

smoother deflection of the power flow. This promises a lot of potential for the Bezier root fillet. Figure 2.4.18 shows the diagram of the dependence of the gear root safety on the Bezier factor  $Be$  for a given gear tooth.

The clearly visible optimum shows a Bezier factor of approximately 0,57. The root load capacity is theoretically increased by 24% compared to conventional values. Figure 2.4.19 shows the shape of the root geometries in dependence on the Bezier factor.

Figure 2.4.20 shows a comparison of the stress and safety distribution of a classic toothing profile with its root optimized variation. The spur gear drive has a module of 6.5 mm as well as

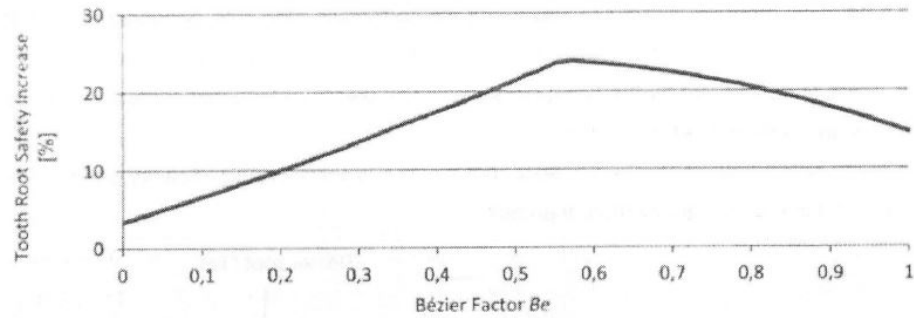


Figure 2.4.18: Influence of the Bezier factor on the gear root safety (source in [3])

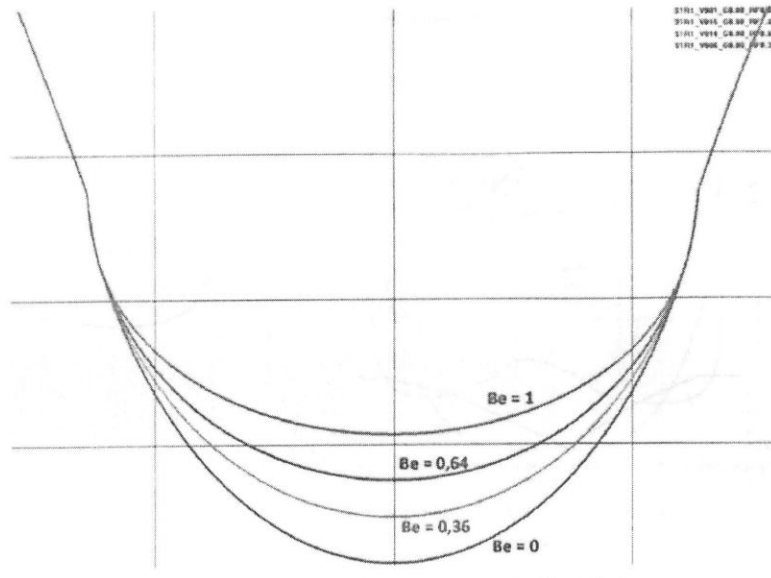


Figure 2.4.19: Shapes of the root fillet depending on the Bezier factor (source in [3])

a pressure angle of 20 degrees. The optimized pinion has 25 teeth and a profile shift coefficient of 0.75. The safety distribution along the tooth space has become significantly smoother in this scenario [3]. The gear root safety is nearly constant for the optimized variation in the large area around the minimum.

The location of the minimum gear root safety has not changed as a result of the new root geometry. The load increment generated by the Bezier root fillet is thus comparable with that of a bionic root contour. Calculations have demonstrated that there is no difference between the two root optimization options.

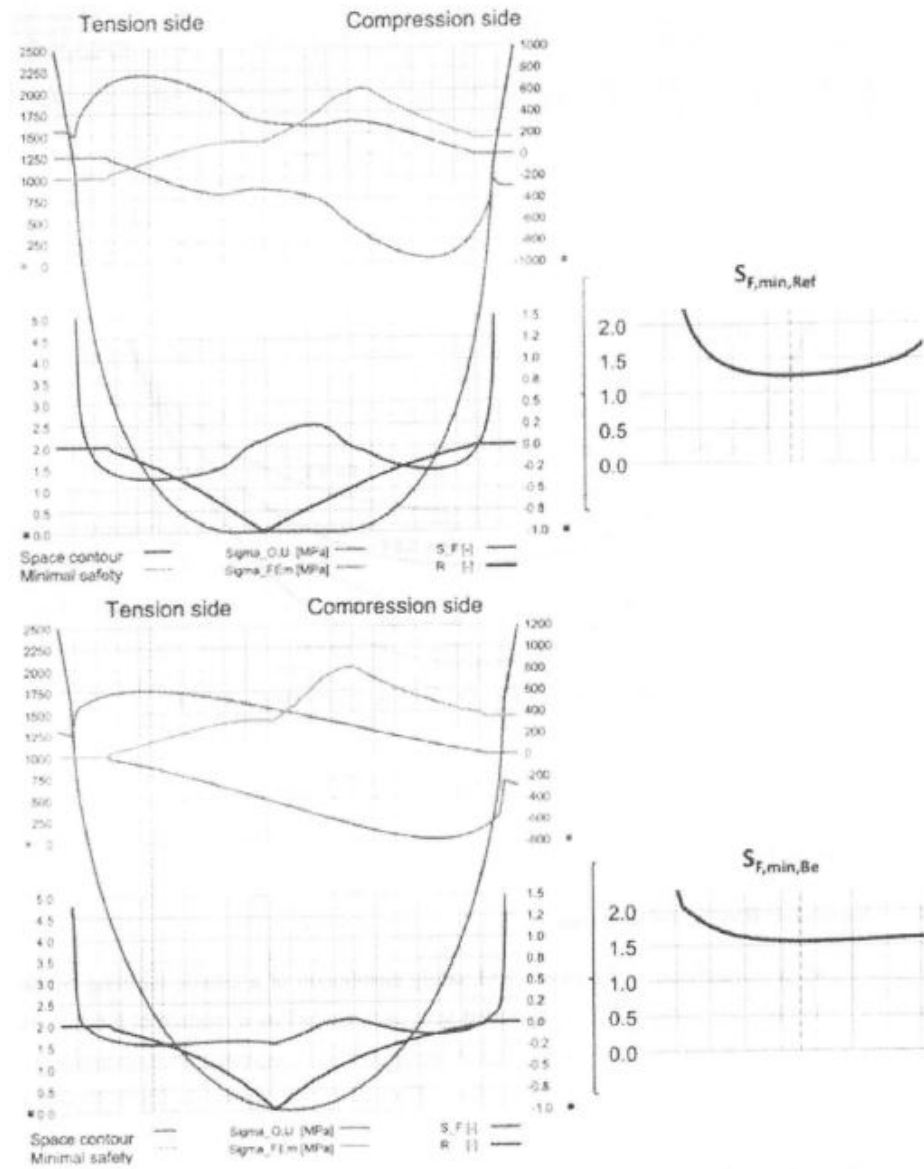


Figure 2.4.20: Load distribution for a classic toothing profile (above) and a Bezier-optimized version (below) (source in [3])

## Chapter 3

# Fundamentals

### 3.1 Introduction

The generation of the tooth surfaces of gears according to the modern theory of gearing allows to simulate real cutting processes from the relative movements between the tool and the gear. The conventional profile of the tooth root or trochoid is obtained in this way as an envelope to the family of circular profiles located at the head of the teeth of the tool. However, the use of form processes instead of generating processes provide more freedom to the root profiles. The modeling of three types of curve to be used as root profiles are presented in this chapter. The three curves are an ellipse, a Hermite curve and a Bezier curve. All of them are defined considering as variables the root radius, the root form radius and the root land width. The equations for each curve are defined as well.

### 3.2 Modeling of an elliptical curve

Figure 3.2.1 shows the variables that control the portion of an ellipse to be used in the tooth root. The active profile is already defined from the cutting process and after applying the modern theory of gearing. The positions of points  $P_0$  and  $P_1$ , initial and final points of the ellipse portion, are controlled through the radii  $\rho_{P_0}$  and  $\rho_{P_1}$  and the width of the root land  $f$ . The point  $R$  serves as a boundary between the angular sectors corresponding to each tooth and defined by the angle  $2\pi/N_g$ , where  $N_g$  is the number of teeth of the gear. This point  $R$  has the same radius as point  $P_1$ .

The major axis of the ellipse passes through point  $P_1$ . The ellipse is univocally defined with the condition that it passes through the points  $P_0$  and  $P_1$  and that the unit tangent  $\mathbf{t}_0$  to the active profile at point  $P_0$  is also tangent to the ellipse. These conditions allow us to define two equations

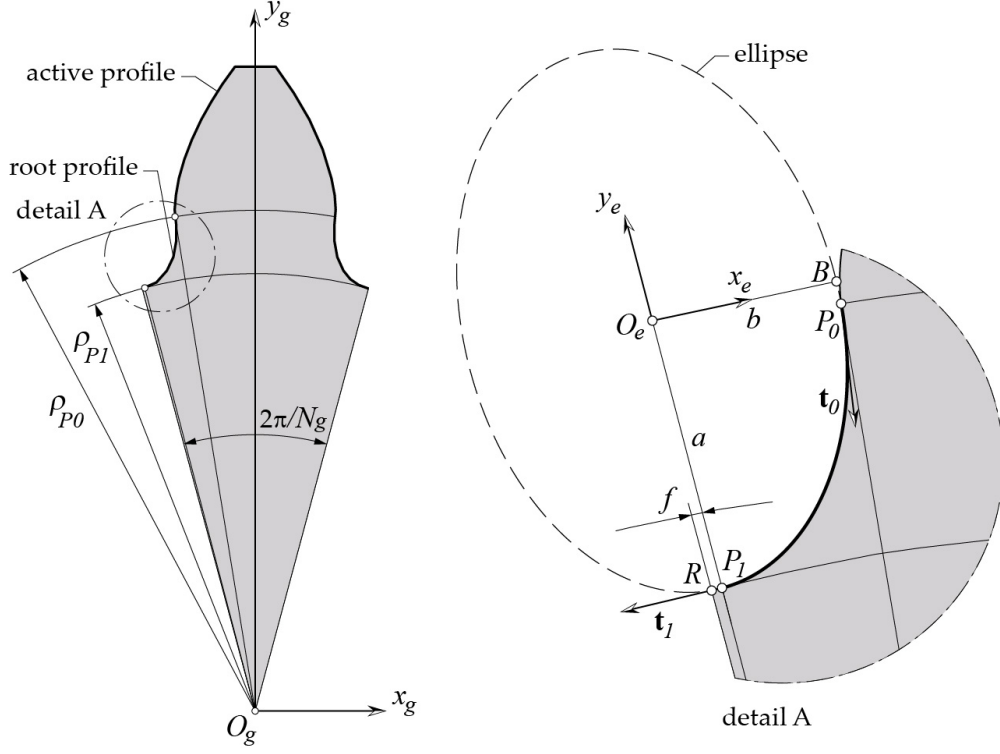


Figure 3.2.1: Modeling of an elliptical curve as tooth root profile

that allow obtaining the lengths of the main semi-axes of the ellipse,  $a$  and  $b$ . These equations are:

$$1 - \frac{x_e^{(P_0)}}{b^2} - \frac{y_e^{(P_0)}}{a^2} = 0 \quad (3.2.1)$$

$$\frac{t_{0ex}}{t_{0ey}} + \left(\frac{a}{b}\right)^2 \frac{x_e^{(P_0)}}{y_e^{(P_0)}} = 0 \quad (3.2.2)$$

Here,  $(x_e^{(P_0)}, y_e^{(P_0)})$  are the coordinates of the point  $P_0$  in the system  $S_e$ , and  $(t_{0ex}, t_{0ey})$  are the components of the vector  $\mathbf{t}_0$  in the system  $S_e$ . The vector position of the point  $P_0$  and the unit tangent  $\mathbf{t}_0$  can be determined initially in a local coordinate system,  $S_g$ , rigidly connected to the gear. Indeed, if the modern gear theory allows defining the active profile of the tooth as  $\mathbf{r}_g(u) = (x_g(u), y_g(u))$  in the system  $S_g$ , where  $u$  is the parameter of the profile, the following condition allows determining the parameter  $u$  corresponding to point  $P_0$

$$\sqrt{(x_g(u^{(P_0)}))^2 + (y_g(u^{(P_0)}))^2} - \rho_{P_0} = 0 \quad (3.2.3)$$

and the following expression allows to obtain the unit tangent in  $P_0$

$$\mathbf{t}_{0g} = \frac{\frac{\partial \mathbf{r}_g}{\partial u} \big|_{u=u^{(P_0)}}}{\left| \frac{\partial \mathbf{r}_g}{\partial u} \big|_{u=u^{(P_0)}} \right|} \quad (3.2.4)$$

Applying then a transformation of coordinate systems from system  $S_g$  to system  $S_e$ , it is possible to obtain the coordinates of  $P_0$  and the unit tangent  $\mathbf{t}_0$  in the system  $S_e$

$$\mathbf{r}_e^{(P_0)} = \mathbf{M}_{eg} \mathbf{r}_g(u^{(P_0)}) \quad (3.2.5)$$

$$\mathbf{t}_{0e} = \mathbf{L}_{eg} \mathbf{t}_{0g}(u^{(P_0)}) \quad (3.2.6)$$

$$\mathbf{M}_{eg} = \begin{pmatrix} \cos(\frac{\pi}{N_g} - \frac{f}{\rho_{P_1}}) & \sin(\frac{\pi}{N_g} - \frac{f}{\rho_{P_1}}) & 0 & 0 \\ -\sin(\frac{\pi}{N_g} - \frac{f}{\rho_{P_1}}) & \cos(\frac{\pi}{N_g} - \frac{f}{\rho_{P_1}}) & 0 & -(\rho_{P_1} + a) \\ 0 & 0 & 1 & 0 \\ 0 & 0 & 0 & 1 \end{pmatrix} \quad (3.2.7)$$

where  $\mathbf{L}_{eg}$  is a 3x3 matrix that results from removing the last row and the last column of matrix  $\mathbf{M}_{eg}$ . Once the semi-axes  $a$  and  $b$  of the ellipse have been determined, the definition of the elliptical profile would be given in the system  $S_e$

$$x_e = x_e^{(P_0)} \cos(\pi t/2) \quad (3.2.8)$$

$$y_e = -\sqrt{b^2 - x_e^2} \frac{a}{b} \quad (3.2.9)$$

The elliptical profile in the system  $S_g$  requires the transformation  $\mathbf{r}_g(t) = \mathbf{M}_{ge} \mathbf{r}_e(t) = \mathbf{M}_{eg}^{-1} \mathbf{r}_e(t)$

### 3.3 Modeling of a Hermite curve

The modeling of the tooth root as a Hermite curve has been proposed in [1] and its formulation here follows the same guidelines. However, with respect to the model presented in [1] some variations are introduced. Figure 3.3.2 shows the tooth root profile with a Hermite curve. This is defined from the position of its initial and final points,  $P_0$  and  $P_1$ , and of the tangents  $\mathbf{T}_0$  and  $\mathbf{T}_1$ , where  $\mathbf{T}_0 = w_0 \mathbf{t}_0$  and  $\mathbf{T}_1 = w_1 \mathbf{t}_1$ . Here,  $w_0$  and  $w_1$  are the weights (or modules) of both tangents. The difference with respect to the model presented in [1] consists in being able to vary the radial position of the points  $P_0$  and  $P_1$  through the radii  $\rho_{P_0}$  and  $\rho_{P_1}$  and of the variable  $f$ .

The Hermite profile in the  $S_g$  system would be given as

$$\mathbf{r}_g(t) = (2t^3 - 3t^2 + 1)\mathbf{r}_g^{(P_0)} + (-2t^3 + 3t^2)\mathbf{r}_g^{(P_1)} + (t^3 - 2t^2 + t)\mathbf{T}_{0g} + (t^3 - t^2)\mathbf{T}_{1g} \quad (3.3.10)$$

$t \in [0, 1]$

The vector position  $\mathbf{r}_g^{(P_0)}$  can be obtained from the value of the profile parameter  $u^{(P_0)}$  that satisfies the relation (3.2.3). The vector position  $\mathbf{r}_g^{(P_1)}$  is obtained as

$$\mathbf{r}_g^{(P_1)} = \begin{pmatrix} -\rho_{P_1} \sin(\frac{\pi}{N_g} - \frac{f}{\rho_{P_1}}) \\ \rho_{P_1} \cos(\frac{\pi}{N_g} - \frac{f}{\rho_{P_1}}) \\ 0 \end{pmatrix} \quad (3.3.11)$$

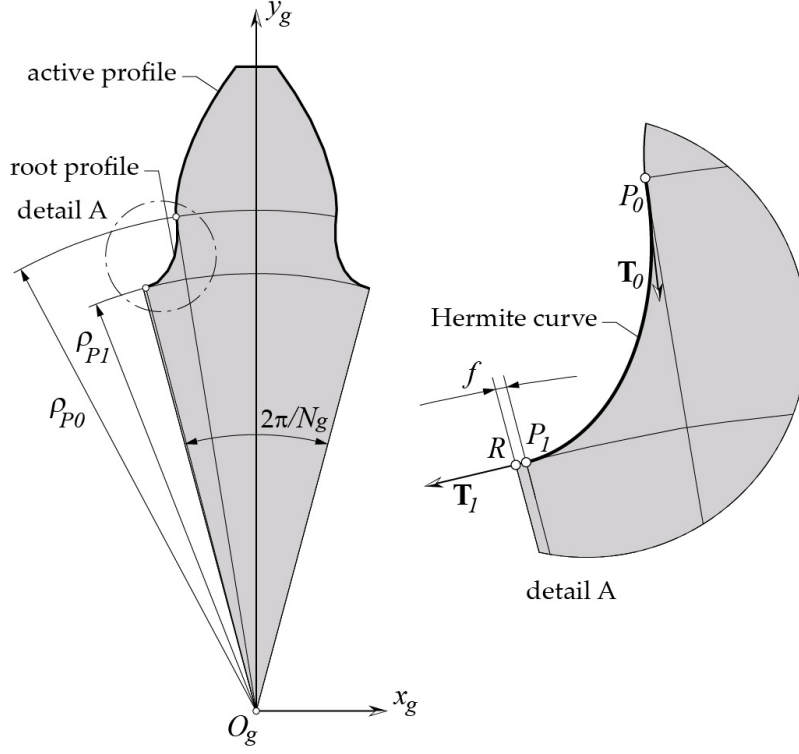


Figure 3.3.2: Modeling of an elliptical curve as tooth root profile.

The tangent  $\mathbf{T}_{0g}$  can be obtained as

$$\mathbf{T}_{0g} = w_0 \frac{\frac{\partial \mathbf{r}_g}{\partial u} \big|_{u=u(P_0)}}{\left| \frac{\partial \mathbf{r}_g}{\partial u} \big|_{u=u(P_0)} \right|} \quad (3.3.12)$$

while the tangent  $\mathbf{T}_{1g}$  is obtained as

$$\mathbf{T}_{1g} = w_1 \begin{pmatrix} -\cos\left(\frac{\pi}{N_g} - \frac{f}{\rho_{P_1}}\right) \\ -\sin\left(\frac{\pi}{N_g} - \frac{f}{\rho_{P_1}}\right) \\ 0 \end{pmatrix} \quad (3.3.13)$$

### 3.4 Modeling of a Bezier curve

The modeling of the tooth root with a third-degree Bezier curve is presented in Figure 3.4.3.

Four points  $P_0$ ,  $P'_1$ ,  $P_2$  and  $P_3$  are required to define a third-degree Bezier curve. The position of these four points allow to define the curve as

$$\mathbf{r}_g(t) = (1-t)^3 \mathbf{r}_g^{(P_0)} + 3(1-t)^2 t \mathbf{r}_g^{(P'_1)} + 3(1-t)t^2 \mathbf{r}_g^{(P_2)} + t^3 \mathbf{r}_g^{(P_3)} \quad (3.4.14)$$

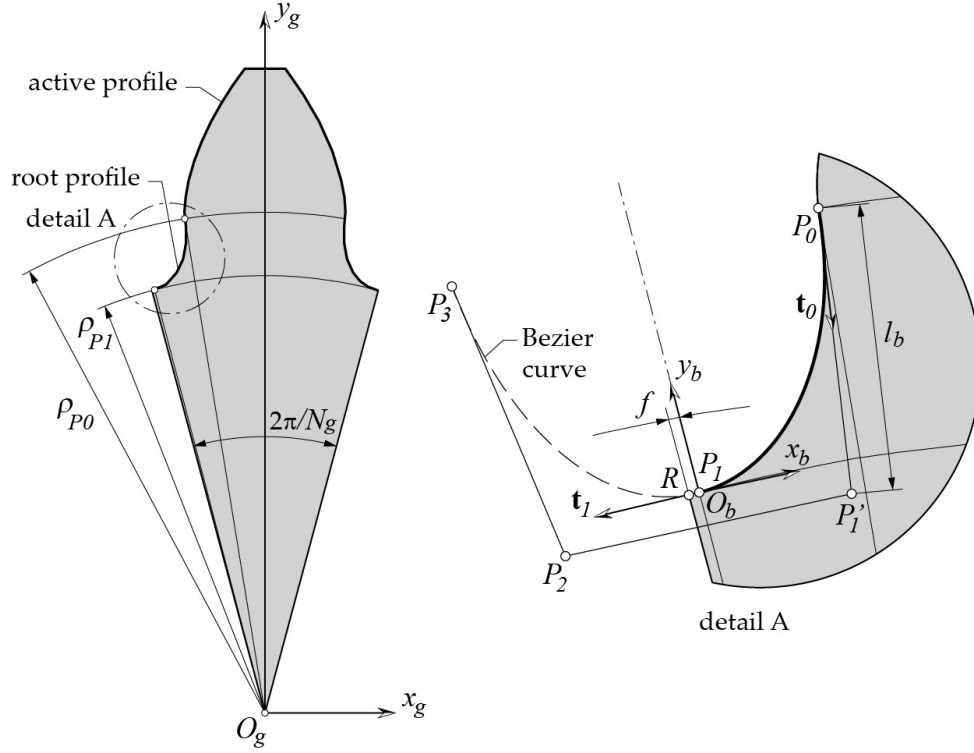


Figure 3.4.3: Figure of Bezier curve

with  $t \in [0, 0.5]$  to define the curve section from point  $P_0$  to point  $P_1$ , which occupies the intermediate position of the curve.

The positions of the points are defined as follows. The vector position  $\mathbf{r}_g^{(P_0)}$  can be obtained from the value of the profile parameter  $u^{(P_0)}$  that satisfies the relation (3.2.3). The vector position  $\mathbf{r}_g^{(P_1)}$  is obtained as

$$\mathbf{r}_g^{(P_1)} = \begin{pmatrix} -\rho_{P_1} \sin\left(\frac{\pi}{N_g} - \frac{f}{\rho_{P_1}}\right) \\ \rho_{P_1} \cos\left(\frac{\pi}{N_g} - \frac{f}{\rho_{P_1}}\right) \\ 0 \end{pmatrix} \quad (3.4.15)$$

The unitary tangent in  $P_0$  will be given as

$$\mathbf{t}_{0g} = \frac{\frac{\partial \mathbf{r}_g}{\partial u} \big|_{u=u^{(P_0)}}}{\left| \frac{\partial \mathbf{r}_g}{\partial u} \big|_{u=u^{(P_0)}} \right|} \quad (3.4.16)$$

Next, a coordinate system  $S_b$  with origin in  $P_1$  is defined with axis  $y_b$  along the radial direction. A coordinate transformation from system  $S_g$  to system  $S_b$  allows to define the position of the points  $P_0$  and  $P_1$ , as well as the tangent  $\mathbf{t}_0$  in the system  $S_b$ .

$$\mathbf{r}_b^{(P_0)} = \mathbf{M}_{bg} \mathbf{r}_g(u^{(P_0)}) \quad (3.4.17)$$

$$\mathbf{r}_b^{(P_1)} = \mathbf{M}_{bg} \mathbf{r}_g^{(P_1)} \quad (3.4.18)$$

$$\mathbf{t}_{0b} = \mathbf{L}_{bg} \mathbf{t}_{0g} \quad (3.4.19)$$

Here,

$$\mathbf{M}_{bg} = \begin{pmatrix} \cos(\frac{\pi}{N_g} - \frac{f}{\rho_{P_1}}) & \sin(\frac{\pi}{N_g} - \frac{f}{\rho_{P_1}}) & 0 & 0 \\ -\sin(\frac{\pi}{N_g} - \frac{f}{\rho_{P_1}}) & \cos(\frac{\pi}{N_g} - \frac{f}{\rho_{P_1}}) & 0 & -\rho_{P_1} \\ 0 & 0 & 1 & 0 \\ 0 & 0 & 0 & 1 \end{pmatrix} \quad (3.4.20)$$

and  $\mathbf{L}_{bg}$  is a 3x3 matrix that results from removing the last row and the last column of the  $\mathbf{M}_{bg}$  matrix. The determination of the point  $P'_1$  in the  $S_g$  system requires solving a system of two equations to obtain the two unknowns  $\mathbf{r}_g^{(P'_1)} = (x_g^{(P'_1)}, y_g^{(P'_1)}, 0, 1)^T$ . A coordinate transformation from the  $S_g$  system to the  $S_b$  system allows defining such vector in system  $S_b$

$$\mathbf{r}_b^{(P'_1)} = \mathbf{M}_{bg} \mathbf{r}_g^{(P'_1)} \quad (3.4.21)$$

Taking into account also that the points  $P_2$  and  $P_3$  occupy positions symmetrical with respect to the axis  $y_b$  to the points  $P'_1$  and  $P_0$ , respectively,

$$x_b^{(P_2)} = -x_b^{(P'_1)} \quad (3.4.22)$$

$$y_b^{(P_2)} = y_b^{(P'_1)} \quad (3.4.23)$$

$$x_b^{(P_3)} = -x_b^{(P_0)} \quad (3.4.24)$$

$$y_b^{(P_3)} = y_b^{(P_0)} \quad (3.4.25)$$

the Bezier curve can then be obtained in the system  $S_b$  as a function of these two unknowns  $(x_g^{(P'_1)}, y_g^{(P'_1)})$

$$\mathbf{r}_b(t) = (1-t)^3 \mathbf{r}_b^{(P_0)} + 3(1-t)^2 t \mathbf{r}_b^{(P'_1)} + 3(1-t) t^2 \mathbf{r}_b^{(P_2)} + t^3 \mathbf{r}_b^{(P_3)} \quad (3.4.26)$$

As the tangent to the Bezier curve at  $t = 0$  is given by

$$\frac{\partial \mathbf{r}_b}{\partial t} \Big|_{t=0} = -3\mathbf{r}_b^{(P_0)} + 3\mathbf{r}_b^{(P'_1)} \quad (3.4.27)$$

and must be parallel to  $\mathbf{t}_{0b}$ , the two conditions that must satisfy the two unknowns are

$$r_{by}(t = 0, 5) = 0 \quad (3.4.28)$$

$$\frac{x_b^{P'_1} - x_b^{P_0}}{y_b^{P'_1} - y_b^{P_0}} = \frac{t_{0bx}}{t_{0by}} \quad (3.4.29)$$

# Chapter 4

## Methodology

### 4.1 Procedure for the analyses

This chapter describes the methodology used to carry out the analyses proposed in the following study. The program used to perform the analyses is IGD. The initial screen of this program is shown in the Figure 4.1.1.

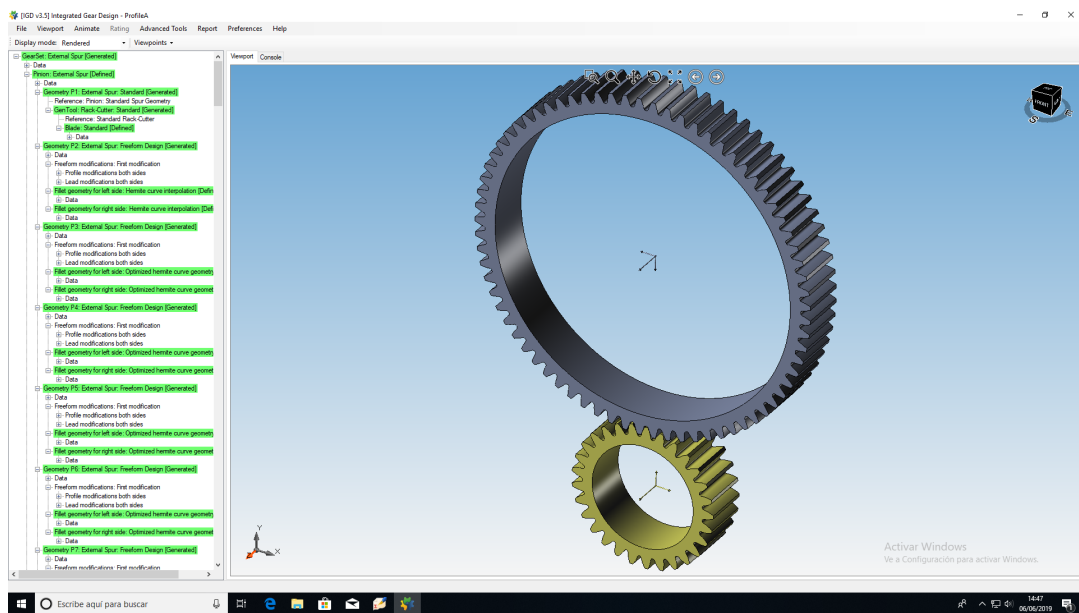


Figure 4.1.1: Initial screen of IGD software

The variables of the pinion are defined in the Figure 4.1.2:

Furthermore, it is also possible to define later some additional conditions. Figure 4.1.3 shows the screen of the program where it is possible to modify the design of the tooth surfaces.

Definition of External Spur Gear (Pini... X

Reference: External Spur Pinion

Gear Data

Number of teeth: 29

Addendum coef.: 1

Dedendum coef.: 1.25

Profile shift coef.: 0.21743275

Face width [mm]: 70

Rim thickness [mm]: ☐ 15.75

Generating Tool Data

Generating shift coef.: 0.21743275

Presentation Data

Number of teeth to show: 3

☒ Show the whole gear

OK Cancel

Figure 4.1.2: Main data of the pinion

Freeform Design

LEFT SIDE BACK SIDE (TOE) RIGHT SIDE

ROOT TOP ROOT

FRONT SIDE (HEEL)

Customized Flank Modifications

Left side

Profile control points: 15 Input deviations

Lead control points: 11 Import deviations

Custom grid positioning Export deviations

Select: Specific lines Edit

Deviations scale factor 1

Copy to right side ->

Copy to left side <-

Clear deviations

Right side

Profile control points: 15 Input deviations

Lead control points: 11 Import deviations

Custom grid positioning Export deviations

Select: Specific lines Edit

Predefined Flank Modifications

Profile modifications

Tip relief

☐ Selected

Datum length [mm]:

Amount [μm]:

Type: Linear

Root relief

☐ Selected

Datum length [mm]:

Amount [μm]:

Type: Linear

Slope modification

☐ Selected

Amount [μm]:

Location: Tip

Type: Linear

Crowning

☐ Selected

Amount [μm]:

Type: Parabolic

Triangular end relief

☐ Selected

Tip datum length [mm]:

Tip length [mm]:

Tip amount [μm]:

Root datum length [mm]:

Root length [mm]:

Root amount [μm]:

Direction: Back root to front tip

Lead modifications

Front relief

☐ Selected

Datum length [mm]:

Amount [μm]:

Type: Linear

Back relief

☐ Selected

Datum length [mm]:

Amount [μm]:

Type: Linear

Slope modification

☐ Selected

Amount [μm]:

Location: Front

Type: Linear

Crowning

☐ Selected

Amount [μm]:

Type: Parabolic

Flank twist

☐ Selected

Front amount [μm]:

Back amount [μm]:

Sign of flank twist: CCW (Z+)

Apply at left side

Apply at right side

Apply at both sides

OK Cancel

Figure 4.1.3: Freeform design

A circular longitudinal crowing and a linear tip relief was selected in the pinion. Furthermore, you can view and edit the definition of standard reference blade profile (see Figure 4.1.4).

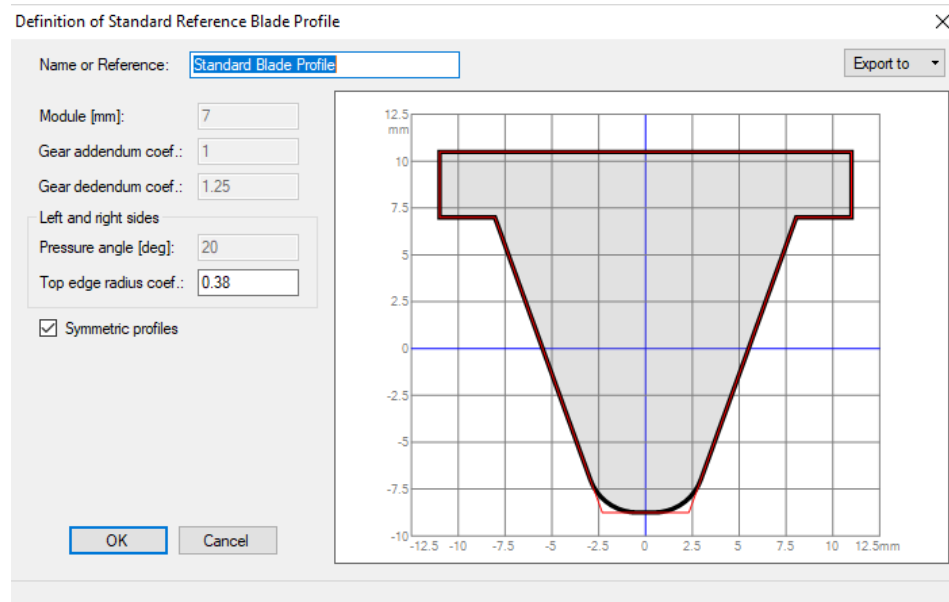


Figure 4.1.4: Definition of standard reference blade profile

Subsequently, the same definition of the gear is made as it is done for the pinion. Figure 4.1.5 shows the screen where it is possible to make this change.

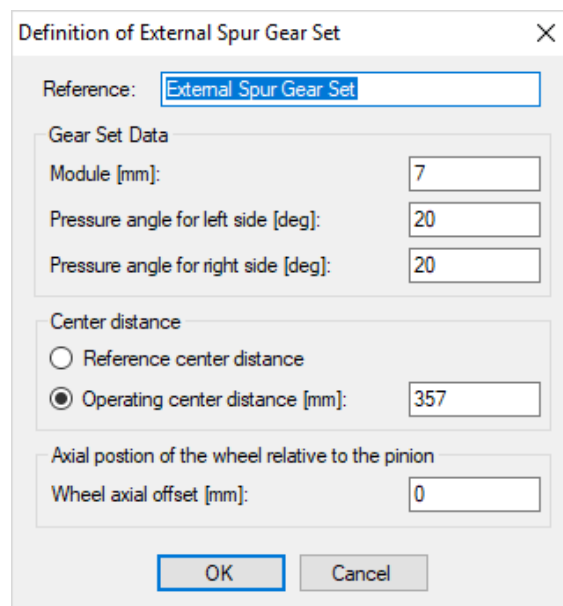


Figure 4.1.5: Definition of external spur gear set

After defining the two basic geometries of the pinion and the gear, the geometry of the pinion just created is copied, in order to be able to make changes and perform different analyses, based on the type of curve used in the fillet of the gear tooth. Figure 4.1.6 shows the screen where these changes can be made.

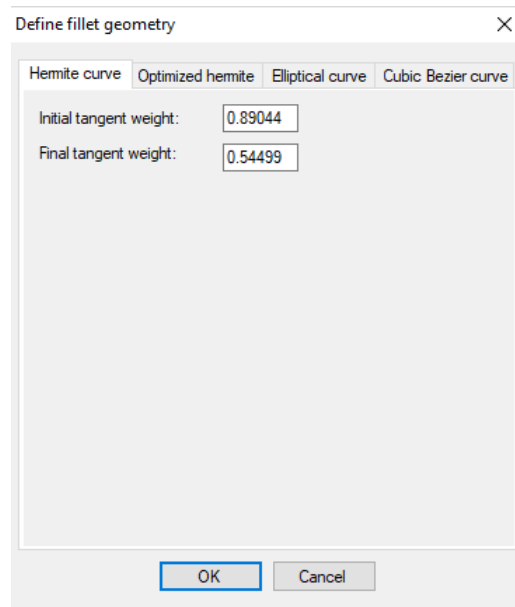


Figure 4.1.6: Definition of the Hermite fillet geometry

In the case of the Hermite curve, the parameters related to this curve, are visualized in Figure 4.1.7.

The parameters that can be changed are:

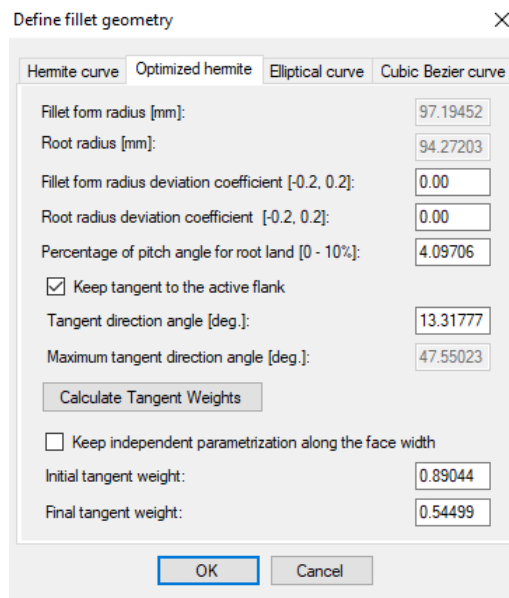
- Fillet from radius deviation coefficient: this value can only vary between -0.2 and +0.2 times the module.
- Root radius deviation coefficient: this value can only vary between -0.2 and +0.2 times the module.
- Percentage of pitch angle for root land: this value can only vary between 0 and 10% of the pitch angle.

In the specific case of Hermite, the values of the tangent weights are the values obtained from the basic Hermite curve.

A similar procedure is performed for the Elliptical curve in Figure 4.1.8.

As it shown in Figure 4.1.8, the parameters that can be modified are:

- Fillet from radius deviation coefficient: this value can only vary between -0.2 and +0.2 times the module.



Define fillet geometry

Hermite curve Optimized hermite Elliptical curve Cubic Bezier curve

Fillet form radius [mm]: 97.19452

Root radius [mm]: 94.27203

Fillet form radius deviation coefficient [-0.2, 0.2]: 0.00

Root radius deviation coefficient [-0.2, 0.2]: 0.00

Percentage of pitch angle for root land [0 - 10%]: 4.09706

☒ Keep tangent to the active flank

Tangent direction angle [deg.]: 13.31777

Maximum tangent direction angle [deg.]: 47.55023

Calculate Tangent Weights

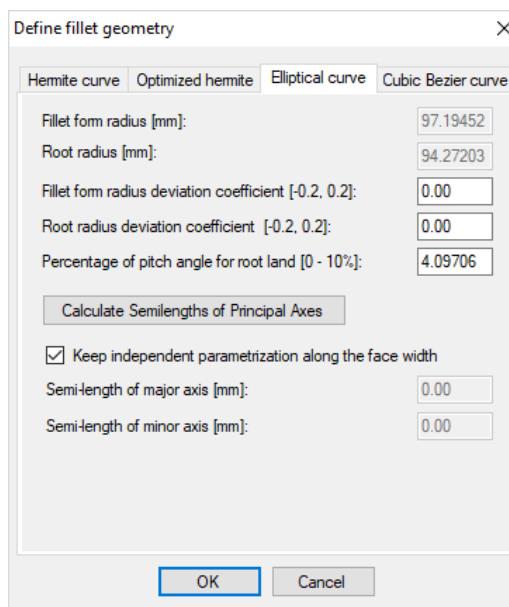
☐ Keep independent parametrization along the face width

Initial tangent weight: 0.89044

Final tangent weight: 0.54499

OK Cancel

Figure 4.1.7: Definition of the optimized Hermite fillet geometry



Define fillet geometry

Hermite curve Optimized hermite Elliptical curve Cubic Bezier curve

Fillet form radius [mm]: 97.19452

Root radius [mm]: 94.27203

Fillet form radius deviation coefficient [-0.2, 0.2]: 0.00

Root radius deviation coefficient [-0.2, 0.2]: 0.00

Percentage of pitch angle for root land [0 - 10%]: 4.09706

Calculate Semilengths of Principal Axes

☒ Keep independent parametrization along the face width

Semi-length of major axis [mm]: 0.00

Semi-length of minor axis [mm]: 0.00

OK Cancel

Figure 4.1.8: Definition of the elliptical fillet geometry

- Root radius deviation coefficient: this value can only vary between -0.2 and +0.2 times the module.
- Percentage of pitch angle for root land: this value can only vary between 0 and 10% of the pitch angle.

Once the parameters required by the analysis have been modified, click on the button "Calculate Semilengths of Principal Axes". It is important to leave the box "Keep independent parametrization along the face width" checked, so that the values of the semi-lengths of principal axes are calculated along the face-width.

A similar procedure is performed for Bezier curve (see Figure 4.1.9).

The image shows a software dialog box titled "Define fillet geometry" with a close button (X) in the top right corner. It features four tabs: "Hemite curve", "Optimized hemite", "Elliptical curve", and "Cubic Bezier curve", with the last one being selected. Below the tabs are five input fields with their current values: "Fillet form radius [mm]: 97.19452", "Root radius [mm]: 94.27203", "Fillet form radius deviation coefficient [-0.2, 0.2]: 0.00", "Root radius deviation coefficient [-0.2, 0.2]: 0.00", and "Percentage of pitch angle for root land [0 - 10%]: 4.09706". A button labeled "Calculate Intermediate Point Coordinates" is positioned below these fields. Underneath the button is a checked checkbox labeled "Keep independent parametrization along the face width" and a final input field "Distance from initial point to intermediate point [mm]: 0.00". At the bottom of the dialog are "OK" and "Cancel" buttons.

Figure 4.1.9: Definition of the Bezier fillet geometry

Figure 4.1.9 shows the parameters that can be modified:

- Fillet form radius deviation coefficient: this value can only vary between -0.2 and +0.2 times the module.
- Root radius deviation coefficient: this value can only vary between -0.2 and +0.2 times the module.
- Percentage of pitch angle for root land: this value can only vary between 0 and 10% of the pitch angle.

Once the parameters required by the analysis have been modified, click on the button "Calculate Intermediate Point Coordinates". It is important to leave the box "Keep independent parametrization along the face width" checked, so this calculation is made along the face width.

Once the geometries of the gear and pinion have been defined, with the changes in the fillet curve, it is possible to proceed with the analyses. Go down the list of operations on the left of the screen, and click on "Analyses" and after a click with the right button of the mouse, choose the "TCA – FEM Analysis" function. (see Figure 4.1.10)

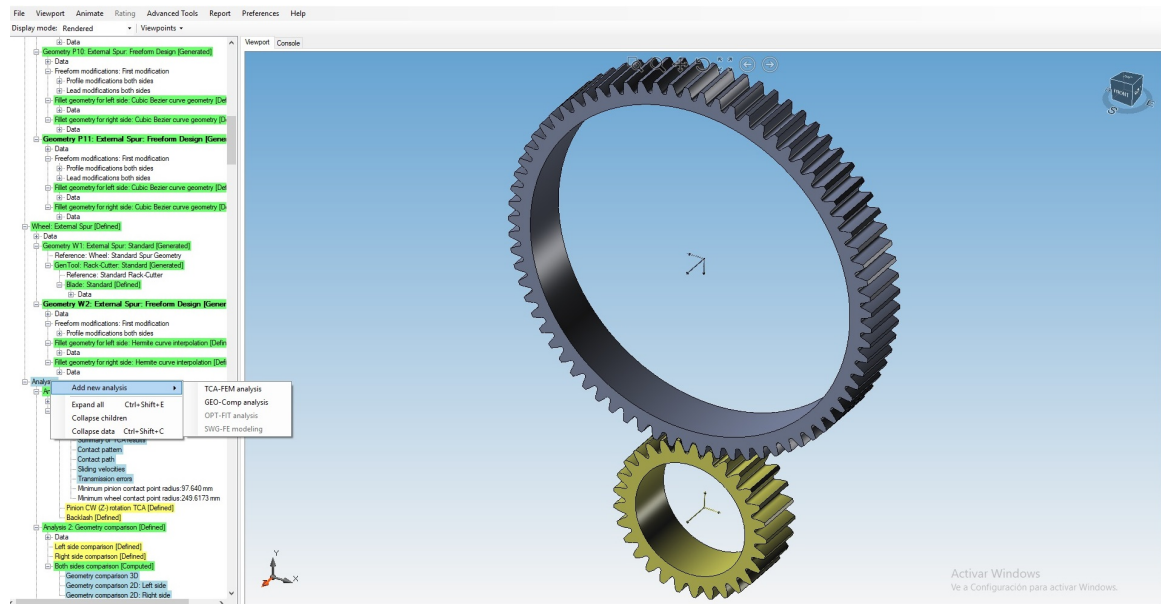


Figure 4.1.10: Analysis selection screen

Once this is done, the type of analysis chosen appears, and the proposed parameters can be modified (see Figure 4.1.11).

In this screen, it is shown which geometry of the pinion and the gear is used for the analysis. In addition, changes can be made to the absolute and relative position of pinion and gear. Once you clicked on "OK", in the screen shown in the Figure 4.1.12 appears:

Here, it is possible to modify different parameters including:

- Number of contact positions;
- Number of pairs of contacting teeth;
- Cycle of meshing;
- Virtual marking compound thickness, expressed in mm;
- Number of point in longitudinal direction;
- Number of points in profile direction;

The dialog box is titled "TCA & FEM Analysis Definition". It has a close button (X) in the top right corner. The "Analysis name or reference:" field contains "TCA & FEM". Under "Gear geometries", "Pinion geometry:" is "Geometry P2: External Spur: Freeform Design" and "Wheel geometry:" is "Geometry W2: External Spur: Freeform Design". There is a "Select geometry" button. Below this are two tabs: "Absolute positioning" (selected) and "Relative positioning". Under "Absolute positioning", there are two sections: "Positioning of the PINION" and "Positioning of the WHEEL". Each section has five input fields: "X displacement [mm]", "Y displacement [mm]", "Z displacement [mm]", "X rotation [deg]", and "Y rotation [deg]". All these fields are set to "0". At the bottom are "OK" and "Cancel" buttons.

Figure 4.1.11: TCA and FEM analysis definition

The dialog box is titled "Tooth Contact Analysis (TCA) Definition". It has a close button (X) in the top right corner. The "Reference:" field contains "TCA". Under "General parameters", there are four input fields: "Number of contact positions:" (21), "Number of pairs of contacting teeth:" (3, with a dropdown arrow), "Cycles of meshing:" (2), and "Virtual marking compound thickness [mm]:" (0.0065). Under "Surface grid definition", there are two input fields: "Number of points in longitudinal direction:" (41) and "Number of points in profile direction:" (41). Under "Transmission presentation", there is one input field: "Show transmission contacting at position:" (11). Under "Initial positioning for the pinion", there are two input fields: "Angle for CCW (Z+) rotation contact [deg]:" (-3.103448275) and "Angle for CW (Z-) rotation contact [deg]:" (3.103448275). At the bottom are "OK" and "Cancel" buttons.

Figure 4.1.12: Tooth contact analysis definition

- Contact position at which the transmission is shown;
- Initial position for the pinion

In the analyses reported in this master thesis work, no changes were made to the system settings. Subsequently, the geometry of the newly defined pinion is processed by clicking on "Pinion *CCW* (Z+) rotation TCA". After that, it is possible to define the finite element model (see Figure 4.1.13).

Figure 4.1.13: Finite element model definition

Here, it is possible to modify different parameters for pinion and wheel:

- Pinion mesh definition;
- Wheel mesh definition;
- Pinion material properties;
- Contact position to analyst;
- Number of pairs of contacting teeth;
- Contact pair type;
- Torque applied to the pinion, expressed in Nm;
- Initial angle of rotation in ABAQUS;
- Torsional deformation of gears;

In this way, it is possible to process the finite element model and export it to the software Abaqus. Once the analysis done, lines of code are used to post-process the results as it is shown in Figure 4.1.14.

```
function RunAndWait([string] $command, [string] $arguments)
{
    $proc = New-Object System.Diagnostics.Process
    $proc.StartInfo.FileName = $command
    $proc.StartInfo.Arguments = $arguments
    $proc.Start()
    $proc.WaitForExit()
}

[System.IO.Directory]::SetCurrentDirectory("C:\FEA\Stefania")
RunAndWait "abaqus" "job=FILE NAME cpus=4 interactive"
RunAndWait "abaqus" "python odbMaxMisesAndCpressV110.py -odb FILE NAME"
```

Figure 4.1.14: Lines of code used to post-process results

Once the analysis on Abaqus has been completed, the results are incorporated in IGD and can be visualized. In this way it is possible to observe the trend of the stress developed in the area of fillet, for pinion and gear. In the following master thesis work the settings shown in the images above have been set.

# Chapter 5

## Results

### 5.1 Numerical examples

The comparison of an elliptical profile, a Hermite curve and a Bezier curve has been made in a transmission of spur gears, whose basic data are shown in a Table 5.1.1. Figure 5.1.1 shows this transmission.

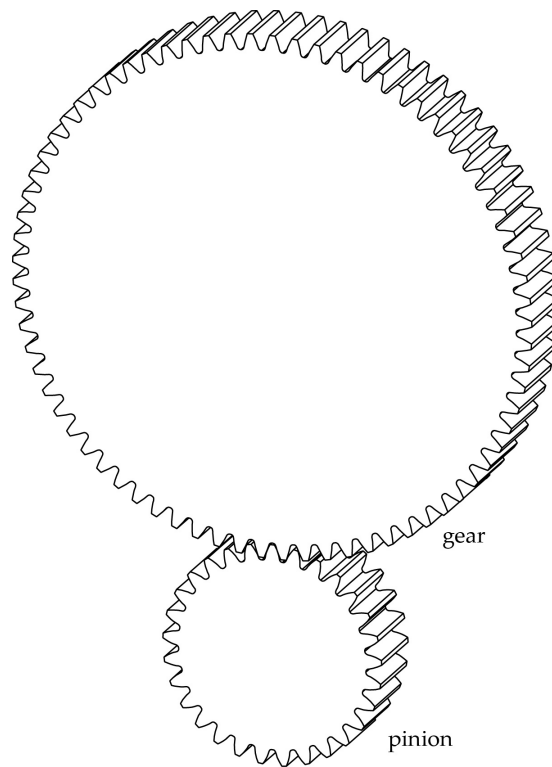


Figure 5.1.1: Example of transmission of spur gears

Table 5.1.1: Table of basic data

Parameter	Pinion	Gear
Number of teeth	29	70
Distance between centers [mm]	357	
Module [mm]	7	7
Face width [mm]	70	70
Normal pressure angle [deg]	20	20
Young's Modulus [GPa]	210	210
Poisson's ratio	0,3	0,3
Applied Torque [Nm]	3100	
Profile Shift Coefficient	0.217	-0.217

Table 5.1.2: Table of the values of the different profiles

Parameter	Profile A	Profile B	Profile C	Profile D
Dedendum	1.25	1.25	1.25	1.40
Root radius coeficient	0.38	0.30	0.25	0.39
Addendum	1.0	1.0	1.0	1.0

We distinguish 4 profiles, A, B, C and D, based on the values of: dedendum, root radius coefficient and addendum, according to the profile ISO 53:1998. (see Table 5.1.2).

Both the surfaces of the teeth of the pinion and those of the gear have profile deviations to reduce the head of the tooth by  $25 \mu\text{m}$  in a length of 3.5 mm from the tip of the tooth and in this way avoid severe contacts on them and reduce contact stress in that area. On the other hand, the surfaces of the teeth of the pinion have flank deviations to center the contact pattern. Lead flank deviation consists of a circular crowning with  $20 \mu\text{m}$  at the front and back edges of the tooth. Figure 5.1.2 shows the profile and flank deviations in pinion and gear.

The tooth root profiles in the geometric models shown in Figure 5.1.1 and Figure 5.1.2 implement Hermite curves where the weights have been determined to reduce the distances between these profiles and those of conventional geometry. Such weights are shown in Table 5.1.3.

Figure 5.1.3 shows the results of a contact analysis in which the pinion and gear tooth surfaces are considered rigid surfaces. The contact pattern is obtained, for each angular position of the pinion, from the approximation of the surfaces of the teeth of the gear to those of the pinion until the distance is minimized, obtaining those points of the gear tooth surface that are at a distance of 0.0065 mm from the pinion tooth surfaces, as contour points of each of the contact patterns

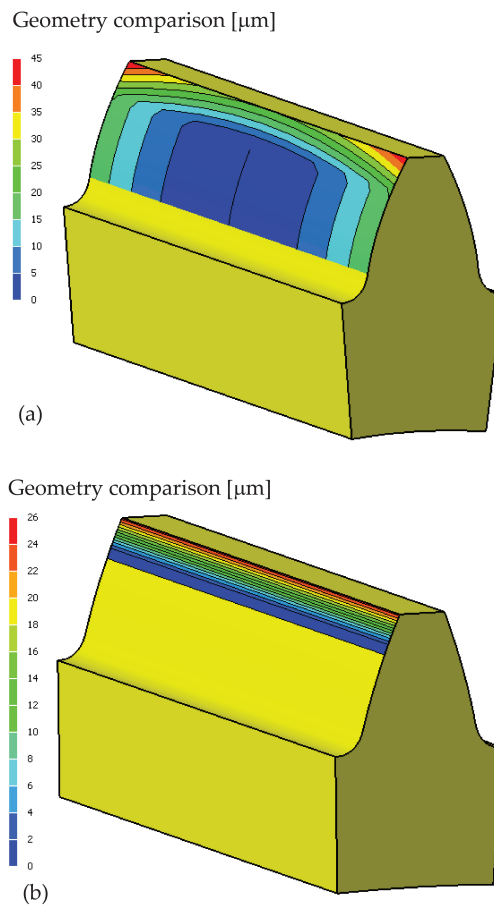


Figure 5.1.2: Comparison of deviations in (a) pinion and (b) gear with respect to a standard geometry

Table 5.1.3: Weights of the unit tangents of the Hermite curve in the tooth root of the geometries with profile and flank deviations

Weights	Pinion	Gear
$w_0$	0.891	0.956
$w_1$	0.545	0.487

between pinion and gear. The transmission errors obtained in this gear drive are null, as the tip relief does not exceed the highest single tooth contact point. The actual size of the contact pattern will be obtained after an analysis by the finite element method.

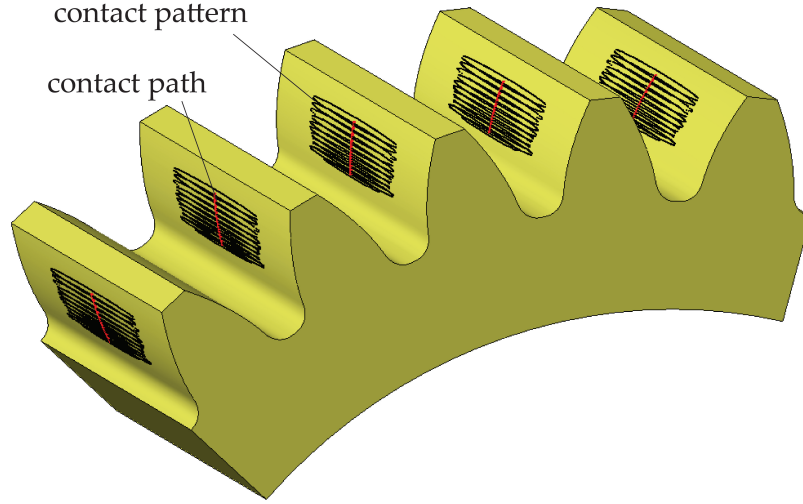


Figure 5.1.3: Contact path and contact patterns on the pinion tooth surfaces

Finite element models are created on the geometric model shown in Figure 5.1.1 and considering the results of the contact analysis shown in Figure 5.1.3. Figure 5.1.4 shows a finite element model of five pairs of teeth. The material considered is steel with an elastic modulus  $E = 207000 \text{ MPa}$  and a Poisson coefficient of  $\nu = 0.3$ . The characteristics of this finite element model are explained in detail in [4]. The torque applied to the pinion through its reference node was 3100 Nm. While the torque remains applied to the pinion, the gear rotates to the different angular positions to complete more than one meshing cycle of a pair of teeth.

The evolution of the contact pressures is observed in Figure 5.1.5 where the load distribution can be shown between the three central couples of the finite element model (pairs 2, 3 and 4 shown in Figure 5.1.4). For this, a general-purpose program was used to solve the stress analysis [?].

The interest of this work lies, however, in the evolution of the bending stresses (maximum principal stress) in the tooth root along the meshing cycle. Figure 5.1.6 shows the evolution of the bending stresses in the central tooth of the pinion model throughout the meshing cycle when 16 finite elements along the root profile are considered.

Next, the different cases analyzed for the different profiles A, B, C and D are reported.

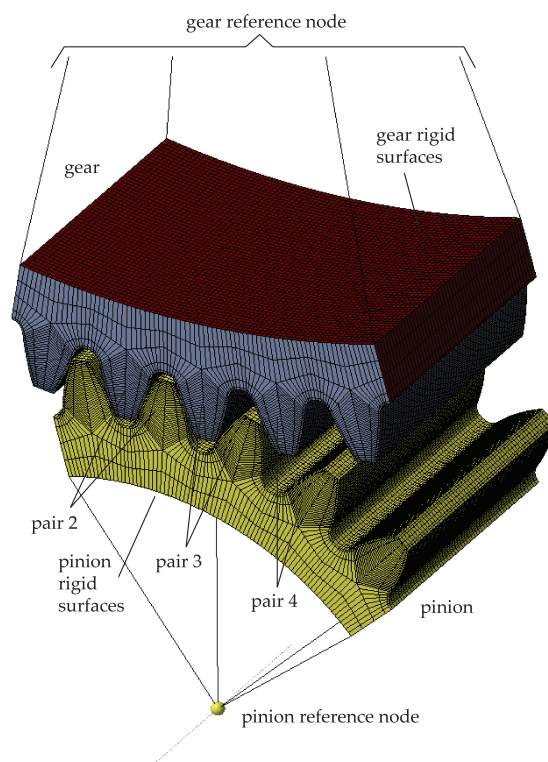


Figure 5.1.4: Finite element model with four pairs of teeth

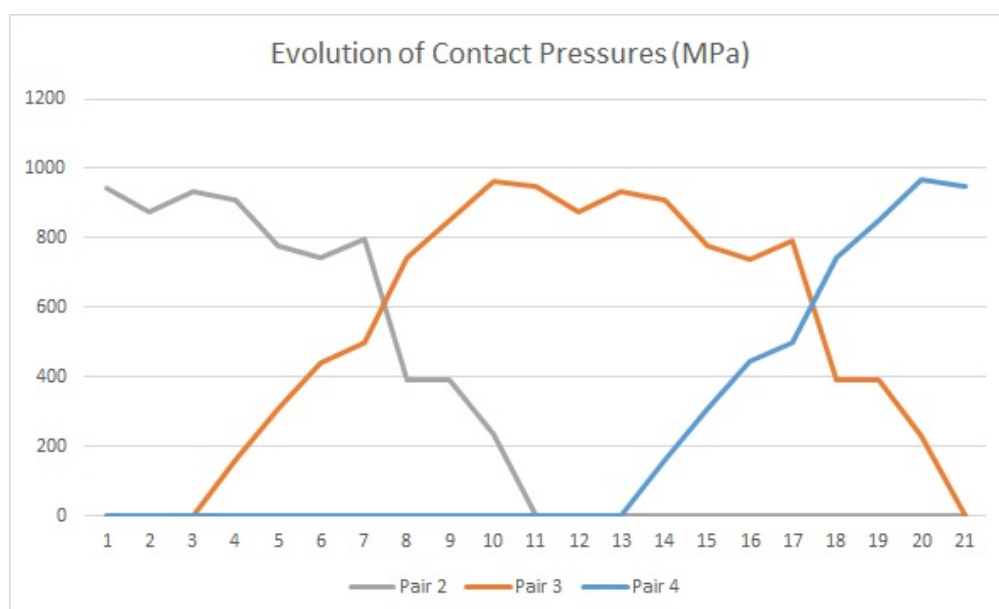


Figure 5.1.5: Evolution of contact pressures throughout a meshing cycle.

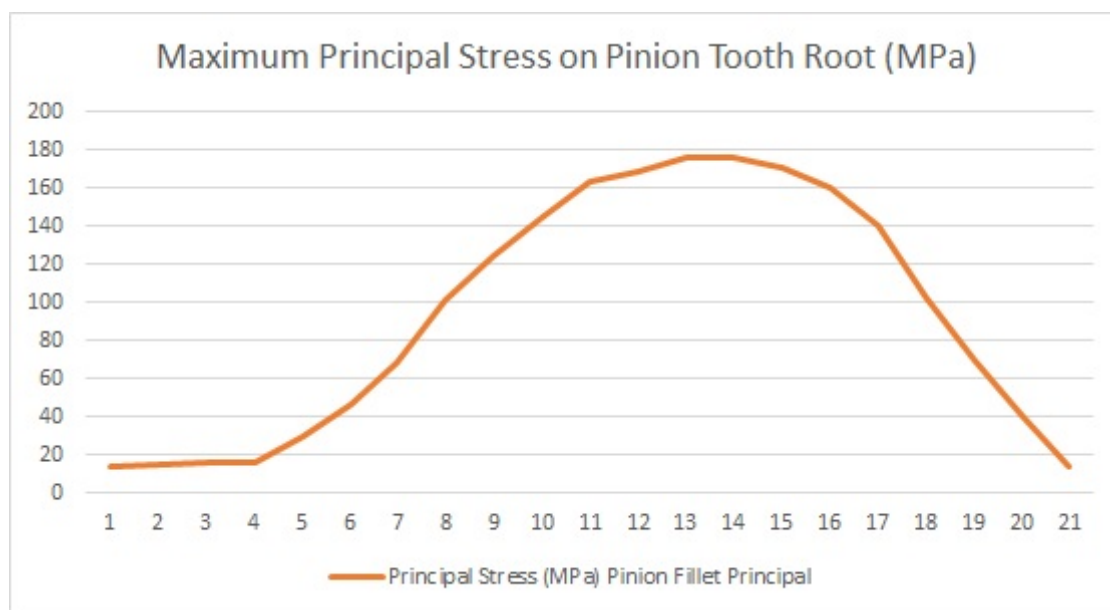


Figure 5.1.6: Evolution of the maximum principal stress in the the central tooth of the pinion during the meshing cycle

## 5.2 ISO profile A

Models considering the ISO profile A with a different number of elements along the root profile of 8, 10, 12, 14, 16 have been considered. Figure 5.2.7 shows the evolution of the maximum value of the maximum principal stress on the fillet of the central tooth of the model when the number of elements is increased. Convergency is observed.

We consider different configurations for all the curves that have been studied: Hermite, Elliptical and Bezier. For all curves, we consider these different cases:

- Configuration 1: Normal configuration, which means that the root land, the fillet form radius and the root radius are not modified respect to their values when the fillet geometry is obtained from a standard rack-curve with the corresponding ISO profile A;
- Configuration 2: Reduction of the root land equal to 1% of the pitch angle;
- Configuration 3: Reduction of the root land equal to 1% of the pitch angle and a fillet form radius deviation coefficient equal to +0.10;
- Configuration 4: Reduction of the root land equal to 1% of the pitch angle and a fillet form radius deviation coefficient equal to +0.20;

Three types of curve, Hermite, Elliptical and Bezier, have been considered in the configurations described above.

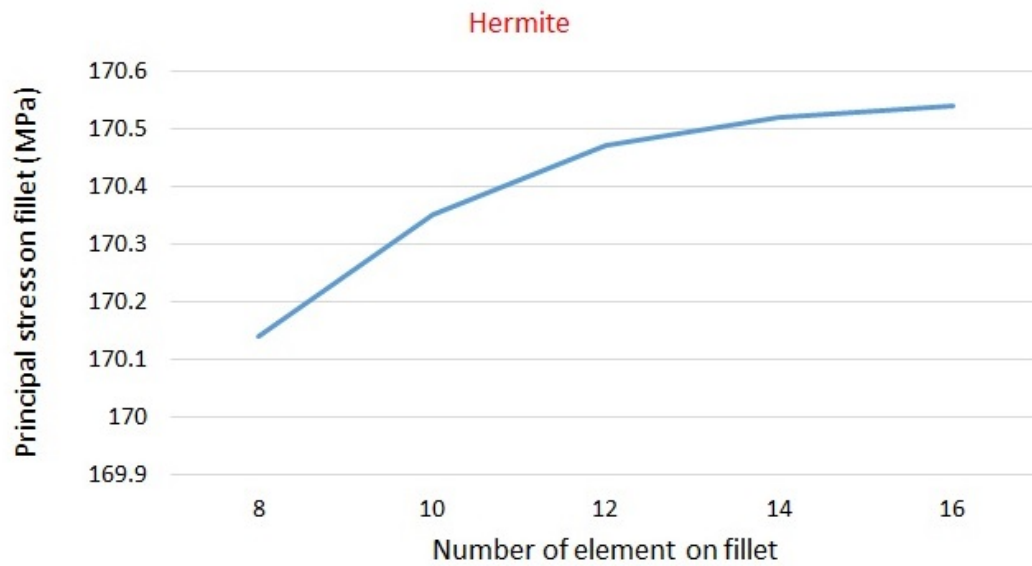


Figure 5.2.7: Maximum principal stress on the fillet for different number of elements

Table 5.2.4: Weights of the unit tangents of the Hermite curve in the tooth root of the geometries with profile and flank deviations

Configuration	$f$ [%]	$\rho_{P0}$ [mm]	$\rho_{P1}$ [mm]
1	4.1	97.195	94.272
2	1	97.195	94.272
3	1	97.195+0.1m	94.272
4	1	97.195+0.2m	94.272

The analyzed cases for the three types of profile are shown in Table 5.2.4. The width of the root land  $f$  is indicated as a percentage of the pitch angle, being

$$f = \frac{\rho_{P1}}{2} \frac{\text{Percentage}}{100} \frac{2\pi}{N_g} \quad (5.2.1)$$

Table 5.2.5 shows the maximum value reached along the cycle of meshing for the maximum principal stress in the fillet for the three types of curve. Figure 5.2.8 shows a decrement in the maximum value reached in the gear cycle of the maximum main voltage by reducing the width of the bottom of the tooth  $f$  and by increasing the radius  $\rho_{P0}$ .

As can be seen from the graph shown, the stress always decreases. The minimum stress obtained is for the condition of a fillet form radius deviation coefficient equal to 0.2 and a percentage of pitch angle for root land equal to 1%. It is observed that this decrease is markedly greater with the

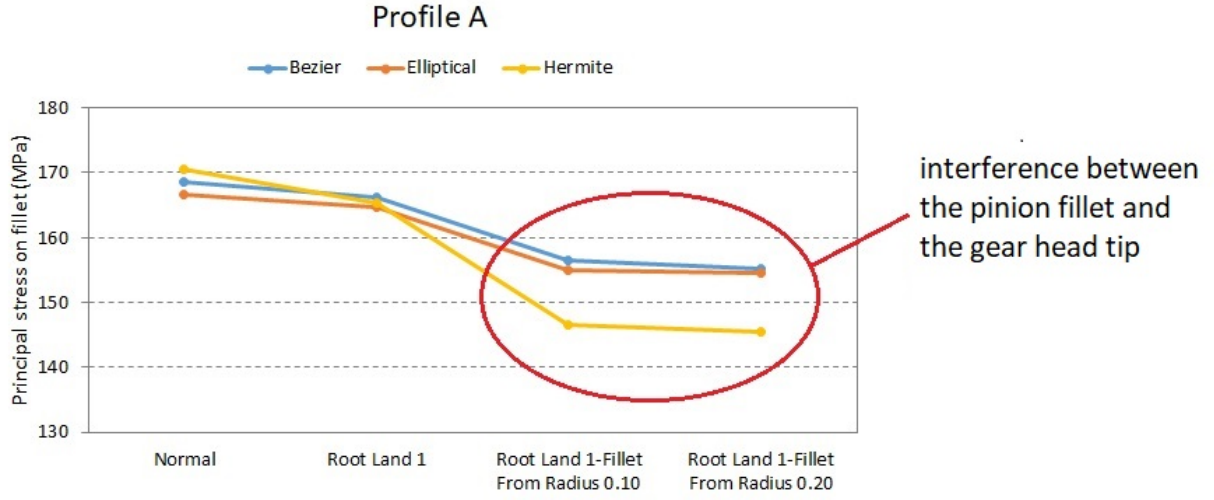


Figure 5.2.8: Principal stress on fillet

Table 5.2.5: Maximum principal stress on the fillet [MPa] for the profile A

Configuration	Hermite	Elliptical	Bezier
1	170.54	166.65	168.68
2	165.43	164.75	166.24
3	146.51	155.08	154.6
4	145.51	154.57	155.27

Hermite curve than with the ellipse and the Bezier curve. Figure 5.2.8 shows a decrease in the maximum value reached in the meshing cycle of the maximum principal stress by reducing the width  $f$  of the root land and by increasing the radius  $\rho_{P0}$ . The increase in  $\rho_{P0}$  is limited by the lowest contact point on the surface of the pinion that contacts the gear tooth surface. This limitation has been taken into account (since the value of  $\rho_{P0}$  must not exceed the maximum value of 98,962 mm obtained from the contact analysis) as well as the evolution of the contact pressures shown in Figure 5.1.5 is not modified in the designs that have been analyzed.

However, the decreases observed for configuration 3 and 4 in Figure 5.2.8 have been made without considering the tooth fillet as a potential contact surface, so they are not real when interference is observed between the tooth fillet of the pinion and the head tip of the gear tooth. The contact pressures shown in Figure 5.1.5 are altered for configuration 3 and 4 if the contact surface is defined not only as the active part of the profile but also with the tooth fillet. It is necessary in these cases and in order to avoid interference to be able to change the direction of the tangent of the tooth fillet at the junction point with the active surface.

Table 5.2.6: Cases analyzed by varying  $f$  and  $\rho_{P_1}$  - Profile A

Configuration	$f$ [%]	$\rho_{P_0}$ [mm]	$\rho_{P_1}$ [mm]
1	4.1	97.193	94.269
2	1	97.193	94.269
3	1	97.193	94.269-0.1m
4	1	97.193	94.269-0.2m

Table 5.2.7: Maximum principal stress on the fillet [MPa]-Profile A

Configuration	Hermite	Elliptical	Bezier
1	170.54	166.65	168.68
2	165.43	164.75	166.24
3	153.06	161.83	163.42
4	158.06	166.87	166.71

Other analyses with the three types of curve, Hermite, elliptical and Bezier, are launched considering:

- Configuration 1: Normal configuration, which means that the root land, the fillet form radius and the root radius are not modified respect to their values when the fillet geometry is obtained from a standard rack-cutter with the corresponding ISO profile;
- Configuration 2: Reduction of the root land equal to 1% of the pitch angle;
- Configuration 3: Reduction of the root land equal to 1% of the pitch angle and a root radius deviation coefficient equal to -0.10;
- Configuration 4: Reduction of the root land equal to 1% of the pitch angle and a root radius deviation coefficient equal to -0.20.

These configurations are shown in Table 5.2.6.

Figure 5.2.9 shows a minimum in the maximum value of the maximum principal stress when decreasing  $\rho_{P_1}$ . This decrease becomes more pronounced in the Hermite curve than in the elliptical and Bezier curves.

The minimum stress obtained is for the condition of root land equal to 1% of the pitch angle and a root radius deviation coefficient equal to -0.10. Comparing the results, a greater reduction in bending stresses is observed by increasing  $\rho_{P_0}$  than by decreasing  $\rho_{P_1}$ . The increase in  $\rho_{P_0}$  is

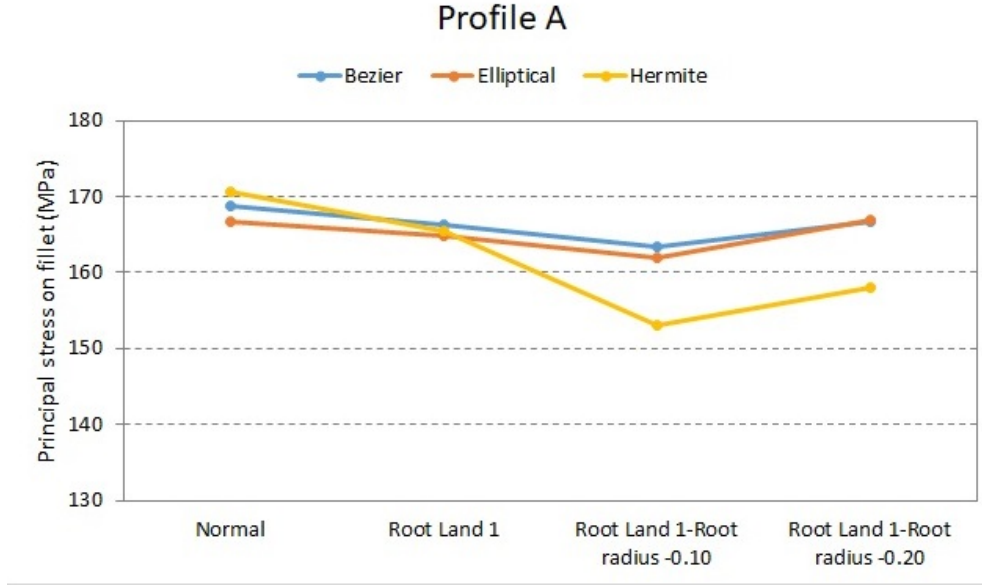


Figure 5.2.9: Principal stress on fillet

limited by the highest contact point on the gear tooth. This limitation has been taken into account (since it has not been possible to increase the value of  $\rho_{P_0}$  any more) as well as the evolution of the contact pressures is not altered in the designs that have been analyzed. The decrease of  $\rho_{P_1}$  is limited by the minimum value reached.

### 5.3 ISO profile B

Figure 5.3.10 shows the maximum value of maximum principal stress on the fillet of the central tooth of the model when the number of elements in the fillet is increased from 8 to 16. Here, the standard geometry with profile B is considered. Similar values of stresses are observed.

Several configurations for all the curves studied, Hermite, elliptical and Bezier curves, are considered:

- Configuration 1: Normal configuration, which means that the root land, the fillet form radius and the root radius are not modified respect to their values when the fillet geometry is obtained from a standard rack-curve with the corresponding ISO profile;
- Configuration 2: Reduction of the root land equal to 1% of the pitch angle;
- Configuration 3: Reduction of the root land equal to 1% of the pitch angle and a fillet form radius deviation coefficient equal to +0.10;

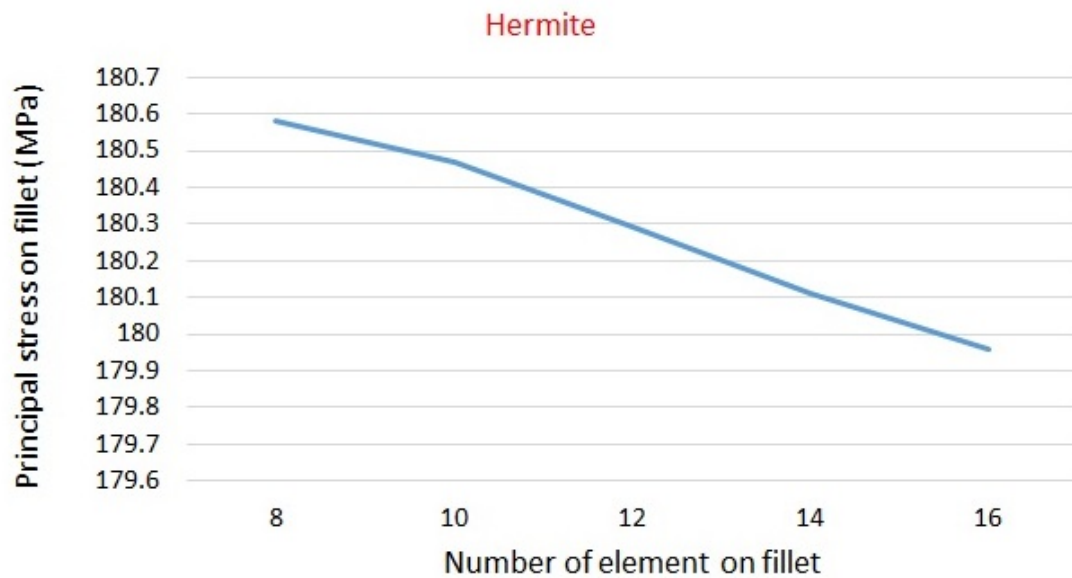


Figure 5.3.10: Principal stress on fillet for number of element on fillet

Table 5.3.8: Cases analyzed by varying  $f$  and  $\rho_{P0}$  - Profile B

Configuration	$f$ [%]	$\rho_{P0}$ [mm]	$\rho_{P1}$ [mm]
1	7.663	96.993	94.272
2	1	96.993	94.272
3	1	96.993+0.1m	94.272
4	1	96.993+0.2m	94.272

- Configuration 4: Reduction of the root land equal to 1% of the pitch angle and a fillet form radius deviation coefficient equal to +0.20.

The analyzed cases for the three types of root profile are shown in Table 5.3.8. The width of the root land  $f$  is indicated as a percentage of the pitch angle and is calculated as indicated in relation (5.2.1).

The results are shown below in a graph and in Table 5.3.9. Figure 5.3.11 shows a decrease in the maximum value reached in the meshing cycle of the maximum principal stress by reducing the width  $f$  of the root land and by increasing the radius  $\rho_{P0}$ .

As can be seen from the graph shown, the stress always decreases, being the behavior similar to profile A. The same problem of interference has been detected for configurations 3 and 4, so modification of the tangent to the fillet at the junction point with the active surface is required to avoid interference.

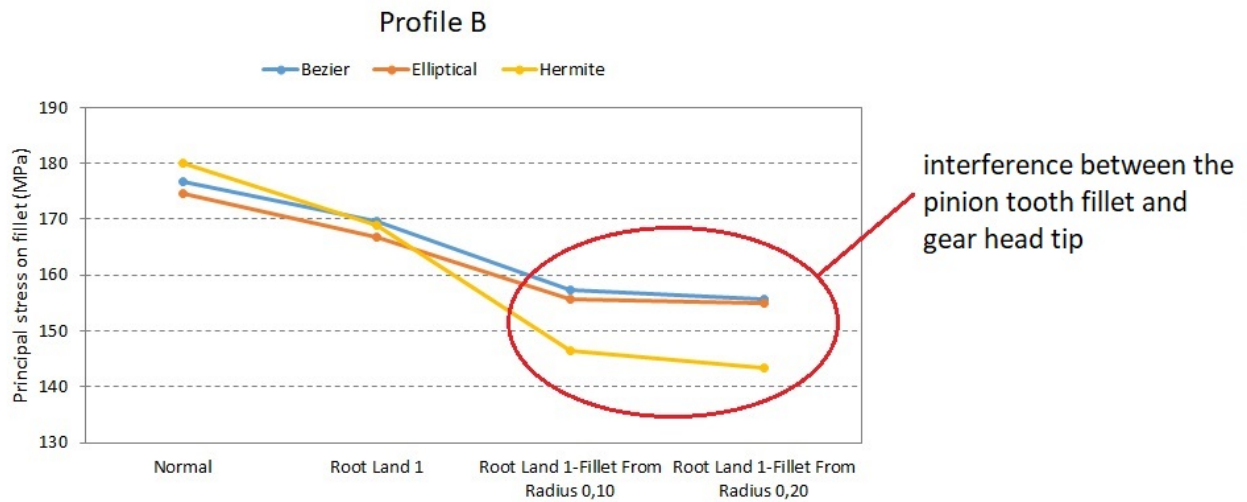


Figure 5.3.11: Principal stress on fillet

Table 5.3.9: Maximum principal stress on the fillet [MPa] - Profile B

Configuration	Hermite	Elliptical	Bezier
1	179.96	174.54	176.80
2	168.95	166.90	169.60
3	146.54	155.64	157.45
4	143.38	154.02	155.74

Some other analyses with the three type of curves, Hermite, elliptical and Bezier, are considered:

- Configuration 1: Normal configuration, which means that the root land, the fillet from radius and the root radius are not modified respect to their values when the fillet geometry is obtained from a standard rack-curve with the corresponding ISO profile;
- Configuration 2: Reduction of the root land equal to 1% of the pitch angle;
- Configuration 3: Reduction of the root land equal to 1% of the pitch angle and a root radius deviation coefficient equal to -0.10;
- Configuration 4: Reduction of the root land equal to 1% of the pitch angle and a root radius deviation coefficient equal to -0.20.

These configurations are illustrated in Table 5.3.10. Table 5.3.11 shows the maximum value of the maximum principal stress reached along the cycle of meshing for each configuration and type of

Table 5.3.10: Cases analyzed by varying  $f$  and  $\rho_{P_1}$  - Profile B

Configuration	$f$ [%]	$\rho_{P_0}$ [mm]	$\rho_{P_1}$ [mm]
1	7.663	96.993	94.272
2	1	96.993	94.272
3	1	96.993	94.272-0.1m
4	1	96.993	94.272-0.2m

curve. Figure 5.3.12 shows graphically these results. A similar behavior is observed than in profile A, reaching a minimum value for a root radius deviation coefficient equal to -0.1.

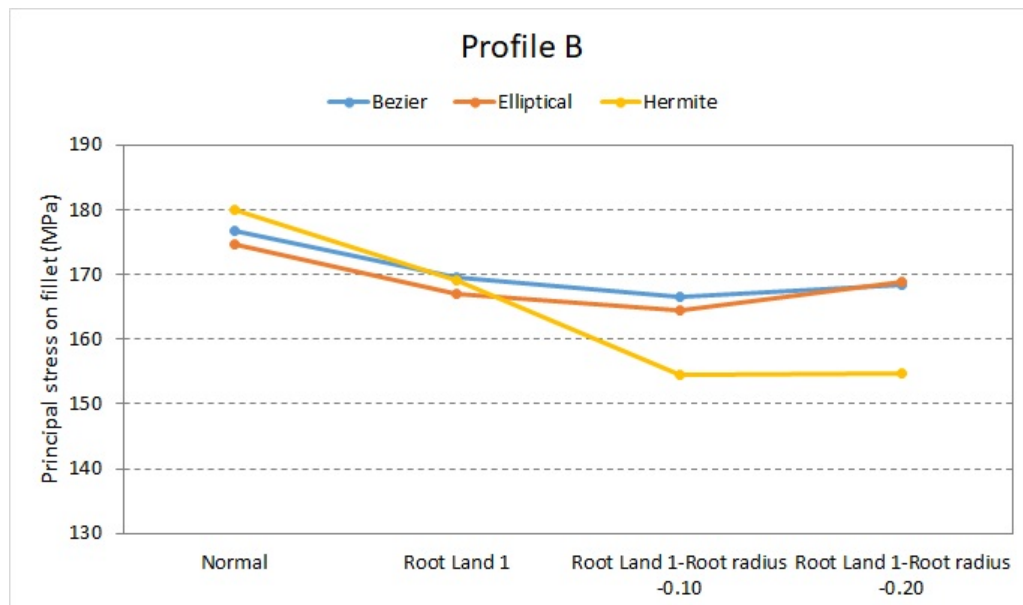


Figure 5.3.12: Principal stress on fillet

## 5.4 ISO profile C

Figure 5.4.13 shows the maximum value, reached along the cycle of meshing, of the maximum principal stress presented on the fillet of the central tooth, for a pinion model with ISO profile C, and when the number of elements in the root profile is increased from 8 to 16. Similar values are observed.

Different configurations for all the curves that have been studied, Hermite, elliptical and Bezier,

Table 5.3.11: Maximum principal stress on the fillet [MPa] - Profile B

Configuration	Hermite	Elliptical	Bezier
1	179.96	174.54	176.80
2	168.95	166.90	169.60
3	154.55	164.35	166.62
4	154.76	168.80	168.28

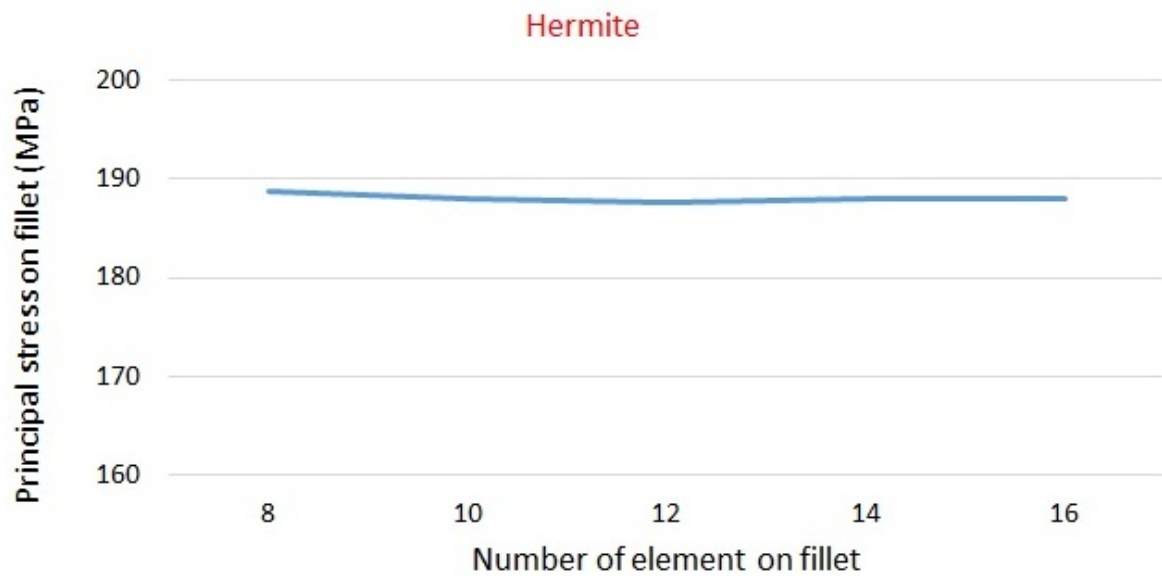


Figure 5.4.13: Principal stress on fillet for number of element on fillet

are considered:

- Configuration 1: Normal configuration, which means that the root land, the fillet form radius and the root radius are not modified respect to their values when the fillet geometry is obtained from a standard rack-curve with the corresponding ISO profile;
- Configuration 2: Reduction of the root land equal to 1% of the pitch angle;
- Configuration 3: Reduction of the root land equal to 1% of the pitch angle and a fillet form radius deviation coefficient equal to +0.10;
- Configuration 4: Reduction of the root land equal to 1% of the pitch angle and a fillet form radius deviation coefficient equal to +0.20;

The cases analyzed for the three types of profile are summarized in Table 5.4.12. The width

Table 5.4.12: Cases analyzed by varying  $f$  and  $\rho_{P0}$  - Profile C

Configuration	$f$ [%]	$\rho_{P0}$ [mm]	$\rho_{P1}$ [mm]
1	9.893	96.873	94.272
2	1	96.873	94.272
3	1	96.873+0.1m	94.272
4	1	96.873+0.2m	94.272

of the root land  $f$  is indicated as a percentage of the pitch angle and is calculated according to relation (5.2.1).

The results of the maximum value of the maximum principal stress are shown below in a graph and in Table 5.4.13. Figure 5.4.14 shows a decrease in the maximum value reached in the meshing cycle of the maximum principal stress by reducing the width of the root land  $f$  and by increasing the radius  $\rho_{P0}$ , as it occurs with ISO profiles A and B.

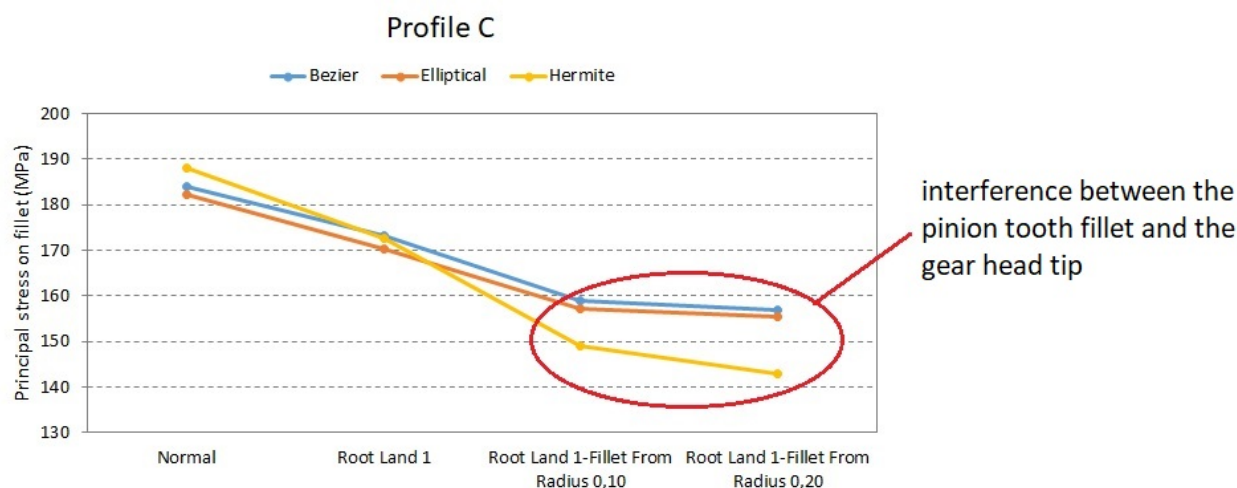


Figure 5.4.14: Principal stress on fillet

Other analyzes with the three types of curve, Hermite, elliptical and Bezier, are based on the following configurations:

- Configuration 1: Normal configuration, which means that the root land, the fillet form radius and the root radius are not modified respect to their values when the fillet geometry is obtained from a standard rack-curve with the corresponding ISO profile;
- Configuration 2: Reduction of the root land equal to 1% of the pitch angle;

Table 5.4.13: Maximum principal stress on the fillet [MPa] - Profile C

Configuration	Hermite	Elliptical	Bezier
1	188.00	182.30	184.10
2	172.69	170.16	173.07
3	149.13	157.25	158.85
4	142.80	155.52	156.81

Table 5.4.14: Cases analyzed by varying  $f$  and  $\rho_{P_1}$  - Profile C

Configuration	$f$ [%]	$\rho_{P_0}$ [mm]	$\rho_{P_1}$ [mm]
1	9.892	96.873	94.272
2	1	96.873	94.272
3	1	96.873	94.272-0.1m
4	1	96.873	94.272-0.2m

- Configuration 3: Reduction of the root land equal to 1% of the pitch angle and a root radius deviation coefficient equal to -0.10;
- Configuration 4: Reduction of the root land equal to 1% of the pitch angle and a root radius deviation coefficient equal to -0.20.

These configurations are illustrated in Table 5.4.14.

Figure 5.4.15 shows a minimum in the maximum value of the maximum principal stress when decreasing  $\rho_{P_1}$ . This decrease becomes more pronounced in the Hermite curve than in the elliptical and Bezier curve. The tendency of the evolution of the stresses is similar to those tendencies that were observed with ISO profiles A and B, although now the minimum value is reached for configuration 4 when the Hermite curve is considered.

Table 5.4.15: Maximum principal stress on the fillet [MPa]-Profile C

Configuration	Hermite	Elliptical	Bezier
1	188.00	182.30	184.10
2	172.69	170.16	173.07
3	157.33	166.05	168.59
4	154.18	169.89	169.71

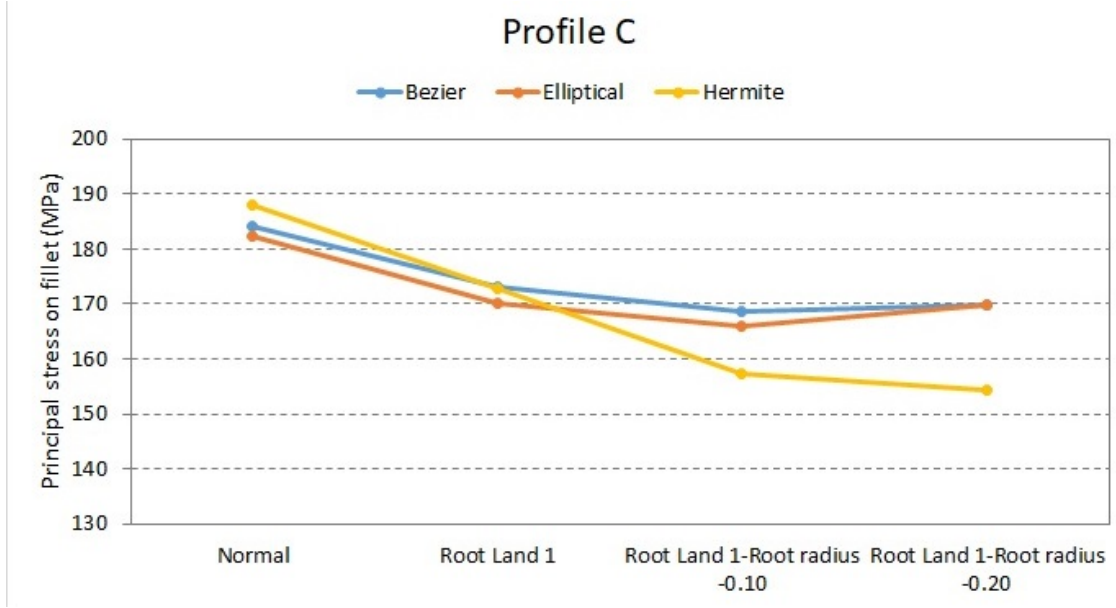


Figure 5.4.15: Principal stress on fillet

## 5.5 ISO profile D

Figure 5.5.16 shows the evolution of the maximum value of the maximum principal stress on the fillet of the central tooth of the model with ISO profile D when the number of elements is increased from 8 to 16. Convergency is observed.

Different configurations for the curves that have been studied, Hermite, elliptical and Bezier, are considered:

- Configuration 1: Normal configuration, which means that the root land, the fillet form radius and the root radius are not modified respect to their values when the fillet geometry is obtained from a standard rack-curve with the corresponding ISO profile D;
- Configuration 2: Fillet form radius deviation coefficient equal to +0.10;
- Configuration 3: Fillet form radius deviation coefficient equal to +0.20;

The cases analyzed for the three types of profile are summarized in Table 5.5.16. The width of the root land  $f$  is indicated as a percentage of the pitch angle and is calculated according to relation (5.2.1).

The results are shown below in a graph and in Table 5.5.17. Figure 5.5.17 shows a decrease in the maximum value reached in the meshing cycle of the maximum principal stress by increasing the radius  $\rho_{P_0}$ .

The graph shows that the stress always decreases although the root land is increased from 0.176% to 1%. The minimum stress obtained is for the condition of fillet form radius deviation

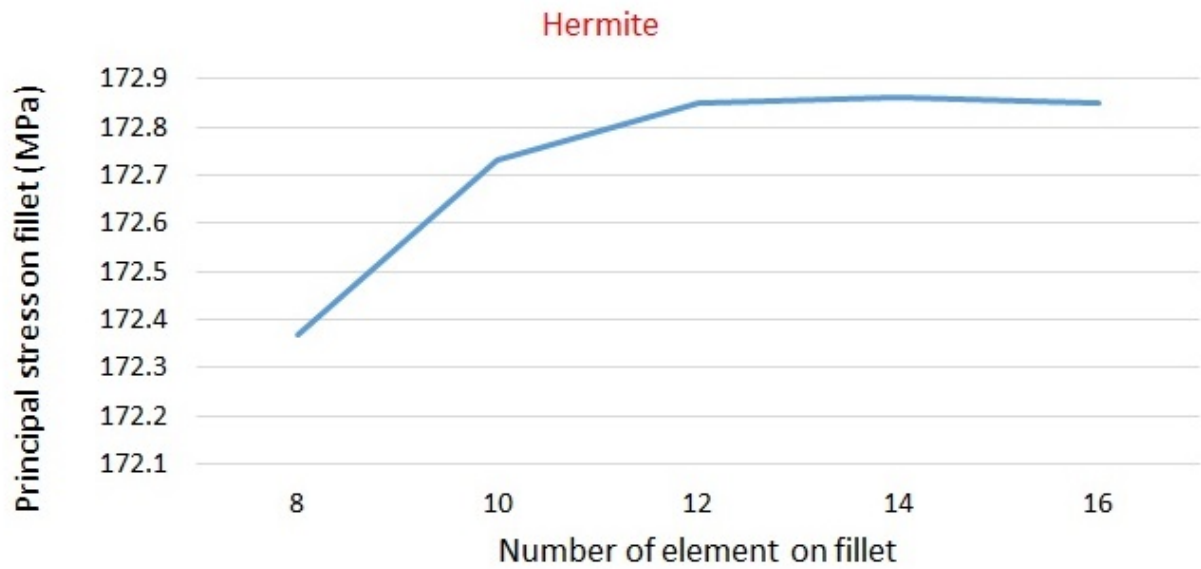


Figure 5.5.16: Principal stress on fillet for number of element on fillet

Table 5.5.16: Cases analyzed by varying  $f$  and  $\rho_{P0}$  - Profile D

Configuration	$f$ [%]	$\rho_{P0}$ [mm]	$\rho_{P1}$ [mm]
1	0.176	96.673	94.272
2	1	96.673+0.1m	94.272
3	1	96.673+0.2m	94.272

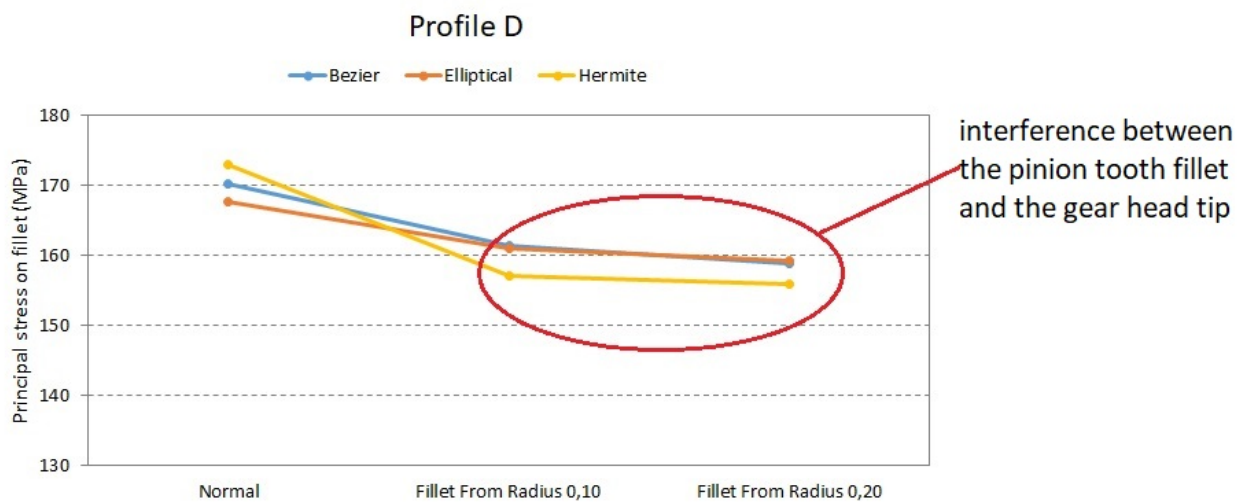


Figure 5.5.17: Principal stress on fillet

Table 5.5.17: Maximum principal stress on the fillet [MPa] - Profile D

Configuration	Hermite	Elliptical	Bezier
1	172.85	167.66	170.30
2	157.01	161.06	161.03
3	155.92	159.22	158.92

Table 5.5.18: Cases analyzed by varying  $f$  and  $\rho_{P_1}$  - Profile D

Configuration	$f$ [%]	$\rho_{P_0}$ [mm]	$\rho_{P_1}$ [mm]
1	0.176	96.673	94.272
2	0.176	96.673	94.272-0.1m
3	0.176	96.673	94.272-0.2m

coefficient equal to +0.2 and a percentage of pitch angle for the root land equal to 1%. It is observed that this decrease is markedly greater with the Hermite curve than with the ellipse and Bezier. The same problem of interference is observed than in the previous ISO profiles. This means that is necessary to change the direction of the tangent to the fillet surface at the junction point with the active tooth surface.

Some other analyzes with the three types of curve, Hermite, Elliptical and Bezier, are considered:

- Configuration 1: Normal configuration, which means that the root land, the fillet form radius and the root radius are not modified respect to their values when the fillet geometry is obtained from a standard rack-curve with the corresponding ISO profile D;
- Configuration 2: A root radius deviation coefficient equal to -0.10;
- Configuration 3: A root radius deviation coefficient equal to -0.20.

These cases are summarized in Table 5.5.18.

Figure 5.5.18 shows a minimum in the maximum value of the maximum principal stress when decreasing  $\rho_{P_1}$  just for the Hermite curve. In an elliptical and a Bezier curve, the stresses always increase. In this case, the increment of the root land from 0.176% of the pitch angle to 1% has a negative effect when decreasing  $\rho_{P_1}$  for elliptical and Bezier root profiles.

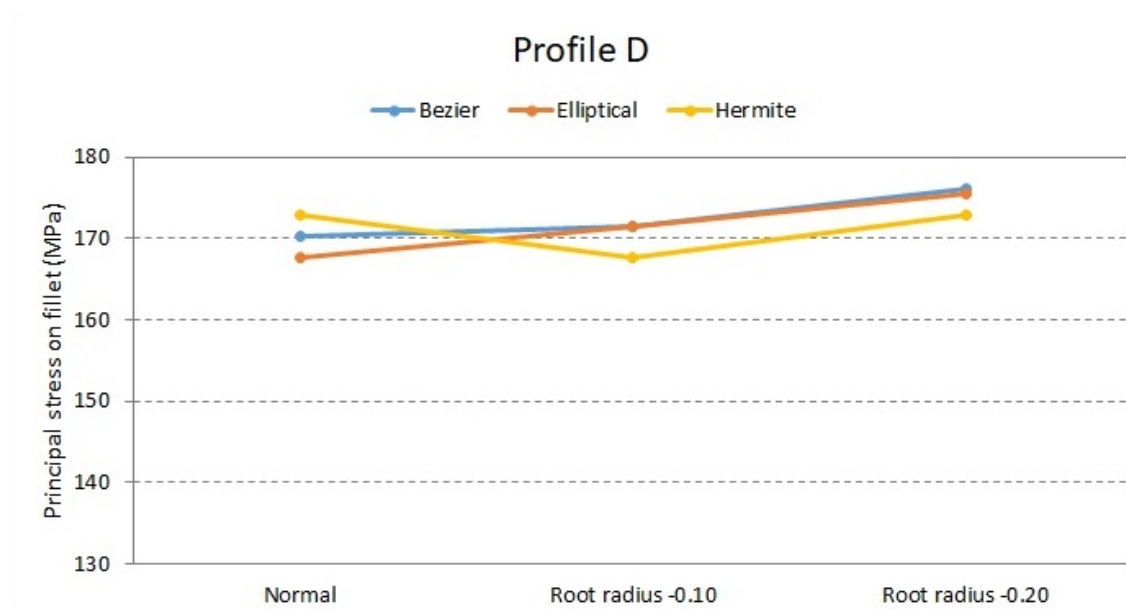


Figure 5.5.18: Principal stress on fillet

Table 5.5.19: Maximum principal stress on the fillet [MPa] - Profile D

Configuration	Hermite	Elliptical	Bezier
1	172.85	167.66	170.30
2	167.69	171.55	171.42
3	172.92	175.45	176.08

## Chapter 6

# Conclusions

The research carried out has led to the following conclusions:

- (1) The use of non-conventional tooth root profiles, based on elliptical profiles, Hermite curve and Bezier curves, allows the maximum value (throughout the meshing cycle) of the maximum principal stress presented in the fillet to be reduced in spur gear drives.
- (2) The use of Hermite curves allows higher reductions than the use of elliptical profiles and Bezier curves, both by increasing the radius of the junction point with the active profile (or fillet form radius), or by decreasing the root radius.
- (3) Both, the increase of the form radius deviation coefficient and the decrease of the root radius deviation coefficient have some limitations that have been taken into account in the present work.
- (4) For the design presented in the present work a maximum reduction of the maximum principal stress has been reached, by increasing the fillet form radius with Hermite curve, in comparison with the reduction when using the ellipse or the Bezier curve. This reduction is different for the four types of considered ISO profiles. Table 6.0.1 shows the reductions obtained for the different analyzed curves and used profiles. The reference geometry for each ISO profile is always the configuration 1 (see Chapter 5).
- (5) Furthermore, a reduction in the case where the root radius decreases has been reached. The reduction is different for the various used profiles. In particular Table 6.0.2 shows the values of the reductions obtained using the different analyzed curves and for the different used profiles.
- (6) The profile with the maximum reduction is certainly the ISO Profile C with Hermite curve when decreasing the root radius and reducing the root land.

Table 6.0.1: Maximum reduction of maximum principal stress when increasing the fillet form radius

Profile type	Hermite	Elliptical	Bezier
Profile A	14.68%	9.36%	9.35%
Profile B	20.33%	14.41%	13.46%
Profile C	24.04%	17.28%	16.59%
Profile D	9.79%	7.88%	8.06%

Table 6.0.2: Maximum reduction of maximum principal stress when decreasing the root radius

Profile type	Hermite	Elliptical	Bezier
Profile A	10.25%	5.11%	4.17%
Profile B	14.12%	8.67%	7.41%
Profile C	17.99%	11.67%	10.32%
Profile D	2.98%	0.75%	0.83%

- (7) The minimum value of maximum principal stress is reached in ISO Profile A with Hermite curve when reducing the root radius.
- (8) These reductions are not extendable to other designs of spur gear drivers since variables such as the number of teeth or the coefficient of displacement of the tool, which affect the shape of the active profile of the teeth, can affect significantly.
- (9) The reductions that have been reached when increasing the fillet form radius require a deep analysis due to the existence of interference between the tip of the gear and the root of the pinion for some configurations.

# Bibliography

- [1] A. Fuentes, P. Iglesias-Victoria, S. Eisele, I. Gonzalez-Perez, "Fillet geometry modeling for non-generated gear tooth surfaces", International Conference on Power Transmissions, Chongqing, China, 2016.
- [2] A. Senders, D.R. Houser, A. Kahraman, J. Harianto, S. Shon, "An experimental investigation of the effect of tooth asymmetry and tooth root shape on root stresses and single tooth bending fatigue life of gear teeth", Proceedings of the ASME Design Engineering Technical Conferences, Washington DC, United States, 2011.
- [3] Z. Roth, J. Opferkuch, J., "High load capacity gear root fillet contour with a Bezier curve", VDI Conference Nr. 2294, Munich, Germany, 2017.
- [4] F.L. Litvin, A. Fuentes. "Gear Geometry and Applied Theory, Second Edition", Cambridge University Press, 2004.
- [5] Dassault Systemes, 2015, "ABAQUS/Standard Analysis User's Guide", Dassault Systemes, Inc., Waltham, MA, Estados Unidos.
- [6] A.L. Kapelevich, Y.V. Shekhtman. "Direct gear design: bending stress minimization". Gear Technology, September/October, pp. 44-47, 2003.
- [7] H. Xiao, W. Zu, W. Zaton. "Fillet shape optimization for gear teeth". Proceedings of the ASME Design Engineering Technical Conferences, Long Beach (CA), DETC2005-84657, 2005.
- [8] M. Shaker. "Optimization of tooth-root profile for maximum load-carrying capacity: spur and bevel gears". Master Engineering Thesis, McGill University, Montreal, 2012.
- [9] A. Akpolat, N. Yildirim, B. Sahin, O. Yildirim, B. Karatas, F. Erdogan. "The effect of asymmetric cutter tip radii on gear tooth root bending stress". AGMA Technical Paper 17FTM06, 2017.
- [10] C. Brecher, C. Löpenhaus, J. Pollaschek, "Potentials of free root fillets in planetary gearbox applications", AGMA Technical Paper 18FTM15, 2018.